university of groningen

Synthesis, Structure, and Magnetic Properties of Copper Oxy-Selenites

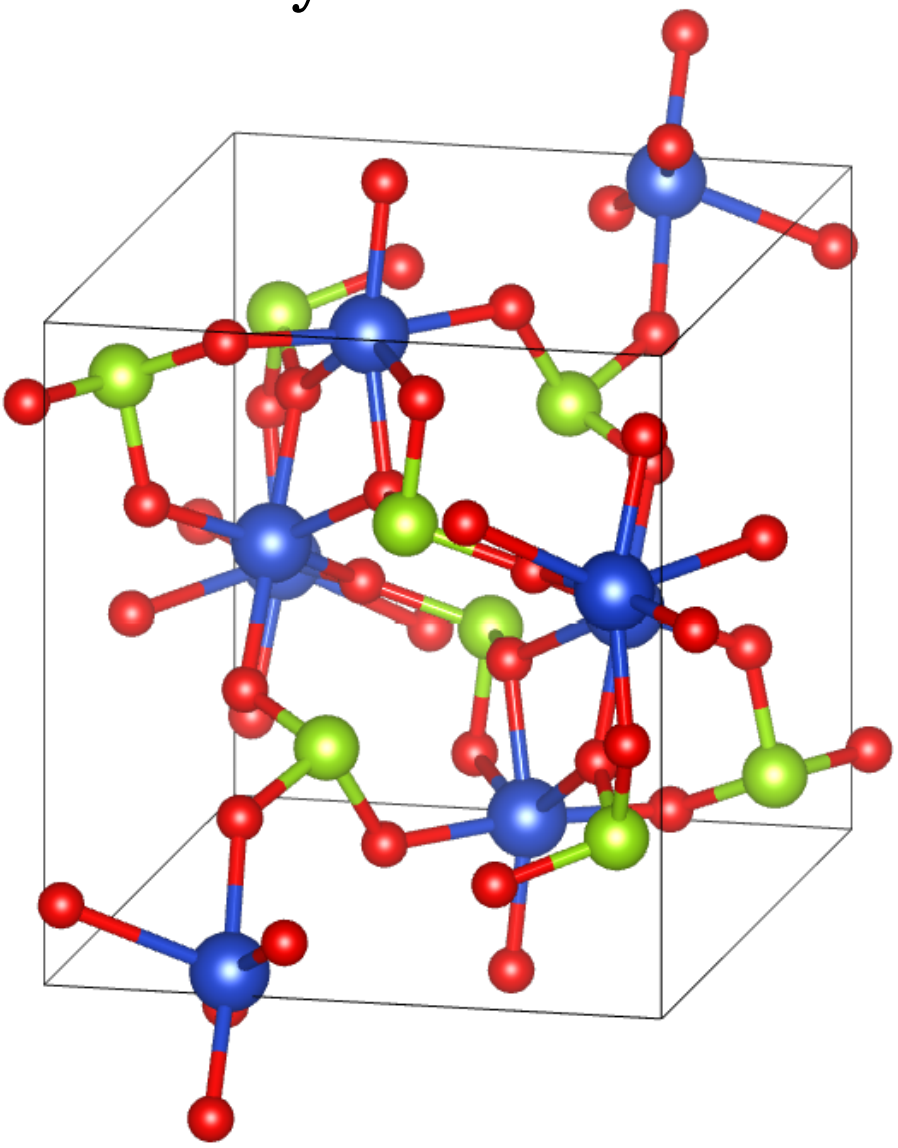

Student: Pepijn Sietsema | s2725886
Daily Supervisor & First Assessor: Dr. G.R. Blake
Second Assessor: Prof. Dr. B. Noheda

Abstract

The goal of this research was to synthesize and analyze the magnetic properties of the triclinic polymorph of the copper oxy-selenite $Cu_4O(SeO_3)_3$. To obtain these results hydrothermal and chemical vapor transport syntheses were performed with differing molar ratios of $Cu(OH)_2$/CuO and SeO_2.

Triclinic $Cu_4O(SeO_3)$ is of interest because of its close relation to the cubic phase of Cu_2OSeO_3, the first and so far only electric insulator able to host magnetic skyrmions. Its magnetic properties have not yet been reported.

Various known copper selenites and copper oxy-selenites were successfully synthesized. Crystalline triclinic $Cu_4O(SeO_3)_3$ was found in the hydrothermal synthesis with a starting molar ratio of 4:3 [$Cu(OH)_2$: SeO_2]. Both the temperature and applied field dependency of the magnetic moment of this compound were investigated for the first time and compared to literature on the skyrmion hosting cubic Cu_2OSeO_3, and the monoclinic $Cu_4O(SeO_3)_3$. Long range antiferromagnetic ordering, with a small ferromagnetic moment, was found with a Néel temperature around T=63K and a ferro- or ferrimagnetic phase above T=48K. Although similar magnetic behavior to Cu_2OSeO_3 was found, the data showed no signs of a transition into a skyrmion phase. At lower temperatures an additional transition was observed around T=16K similar to a transition found in monoclinic $Cu_4O(SeO_3)_3$.

Table of Contents

1 Introduction

Copper selenites, including copper oxy selenites, have been synthesized as early as 1958 during which their various crystal structures were also determined [1][2]. It was however not until much later in 2012 that this family of crystal structures started to regain attention, after the cubic copper oxy-selenite Cu_2OSeO_3 was found to host complex spiraling magnetic structures known as skyrmions [3].

1.1 Magnetic Skyrmions

Magnetic skyrmions are two dimensional solitons consisting of magnetic moments in vortex-like configurations, although they are topologically different from regular vortices. They were first shown to be theoretically possible by Tony Skyrme and were later theorized to exist in non-centrosymmetric magnetic crystals, where so called Dzyaloshinskii–Moriya, or antisymmetric exchange, interactions favor a relative tilt in neighboring magnetic spins that are normally ferromagnetically or antiferromagnetically aligned. This exchange interaction can stabilize magnetic skyrmions and cause multiferroic behavior in the material.

Skyrmions consist of a collection of spins that over a distance reverse in direction, in a fashion analogous to common antiferromagnetic domain walls. The relative rotation of these spins can happen in the radial plane or the tangential plane, giving rise to Neel-type and Bloch-type skyrmions respectively as shown in *Figure 1.1a*. These types of skyrmions are also known as having spiral and hedgehog configurations, which can be visualized when mapping their spin arrangement onto a sphere. In topology these configurations are 'protected', they can only be created and destroyed by specific interactions.

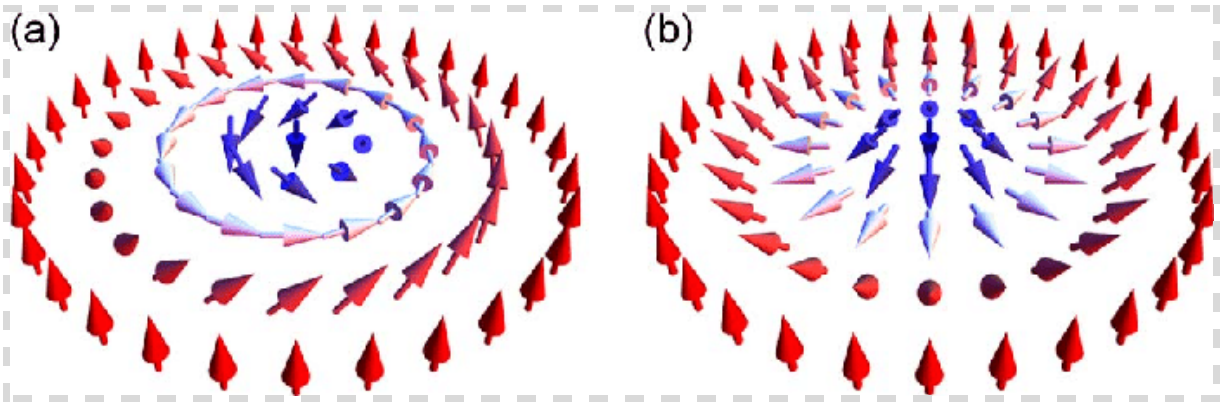

Figure 1.1a: Bloch-type and Néel-type skyrmions. (a) In a Bloch-type skyrmion, the spins rotate in the tangential planes, that is, perpendicular to the radial directions, when moving from the core to the periphery. (b) In a Néel-type skyrmion, the spins rotate in the radial planes from the core to the periphery. [4]

The ability to manipulate these relatively small and stable magnetic configurations is promising for magnetic storage, where the presence or absence of a skyrmion would encode a bit at an incredibly small scale. Their stability as solitons is specifically of interest in the development of racetrack memory, where magnetic domains which encode the bits are pushed along a wire by a small electric current.

Skyrmions have since been observed experimentally in various non-centrosymmetric materials, including FeGe [5], MnSi [6], Cu_2OSeO_3 [3], with skyrmions ranging from 10 nm to 200 nm in size. A multitude of engineered metallic nanolayers have also shown to host skyrmions of larger sizes, in the 100 nm to 10μm range[7][8][9]. More recent studies have also shown the presence of noticeably small skyrmions, ranging from 1 nm to 10 nm, in magnetically frustrated centrosymmetric rare-earth based materials like Gd_2PdSi_3 [10], $GdRu_2Si_2$ [11], $Gd_3Ru_4Al_{12}$ [12], and $EuAl_4$ [13]. The symmetry of the skyrmion lattices were found to represent the underlying crystal lattice and a mechanism involving itinerant electrons has been proposed [14].

1.2 Copper Selenites and Copper Oxy-Selenites

	a [Å]	b [Å]	c [Å]	α [°]	β [°]	γ [°]	Space Group
$CuSeO_3$ I **[15]**	5.965	7.327	5.283	-	-	-	Orthorhombic Pnma
$CuSeO_3$ II **[16]**	5.962	7.010	12.240	-	-	-	Orthorhombic Pcab
$CuSeO_3$ III **[16]**	7.725	8.241	8.502	-	99.12	-	Monoclinic $P2_1/n$
$CuSeO_3$ IV **[16]**	4.736	8.579	10.618	66.69	88.53	88.40	Triclinic $P\bar{1}$
$CuSeO_3 \cdot 2H_2O$ [1]	6.664	9.156	7.369	-	-	-	Orthorhombic $P2_12_12_1$
Cu_2OSeO_3 I **[2]**	8.925	-	-	-	-	-	Cubic $P2_13$
Cu_2OSeO_3 II **[2]**	6.987	5.953	8.429	-	92.17	-	Monoclinic $P2_1/n$
$Cu_4O(SeO_3)_3$ I **[2]**	15.990	13.518	17.745	-	90.49	-	Monoclinic $P2_1/a$
$Cu_4O(SeO_3)_3$ II **[2]**	7.992	8.141	8.391	77.34	65.56	81.36	Triclinic $P\bar{1}$
$Cu_5O_2(SeO_3)_2Cl_2$ I **[17]**	6.047	13.782	5.579	-	95.76	-	Monoclinic $P2_1/c$
$Cu_5O_2(SeO_3)_2Cl_2$ II **[18]**	5.398	8.054	11.128	-	99.26	-	Monoclinic $P2_1/c$
$Cu_9O_2(SeO_3)_4Cl_6$ I **[19]**	14.170	6.262	12.999	-	113.05	-	Monoclinic I2/m
$Cu_9O_2(SeO_3)_4Cl_6$ II **[20]**	12.922	6.262	14.042	-	112.88	-	Monoclinic $P2_1/n$
$Cu_9O_2(SeO_3)_4Cl_6$ III **[21]**	14.942	6.265	12.939	-	120.03	-	Monoclinic C2/m

Table 1.2a: The reported crystal structure parameters of relevant copper selenites and copper oxy-selenites.

In the following section a literature review is given of selected compounds in the copper selenite and copper oxy-selenite families, the focus of this thesis.

1.2.1 Cu_2OSeO_3

The most notable of the copper oxy-selenites is the cubic polymorph of Cu_2OSeO_3, the first and so far only electrically insulating material known to host magnetic skyrmions. The skyrmion phase in bulk Cu_2OSeO_3 is illustrated in *Figure 1.2b* and is located in a small region of the temperature - applied magnetic field phase diagram between temperatures of 55-58K and applied fields of 150-400Oe. In addition to the paramagnetic and ferrimagnetic phases in the phase diagram, two helical structures are also present. The identification of the ferrimagnetic phase is based on powder neutron diffraction [22] and nuclear magnetic resonance [23] studies that suggest that the spins of four Cu^{2+} cations coordinated in a trigonal bipyramidal fashion to oxygen are aligned antiparallel to those of twelve Cu^{2+} cations coordinated in a square pyramidal fashion, see *Figure 1.2c*. [3]

Cu_2OSeO_3 also has a reported monoclinic polymorph, of which only the structural properties are known [2]. This structure has not been reported on since it was first identified in 1986.

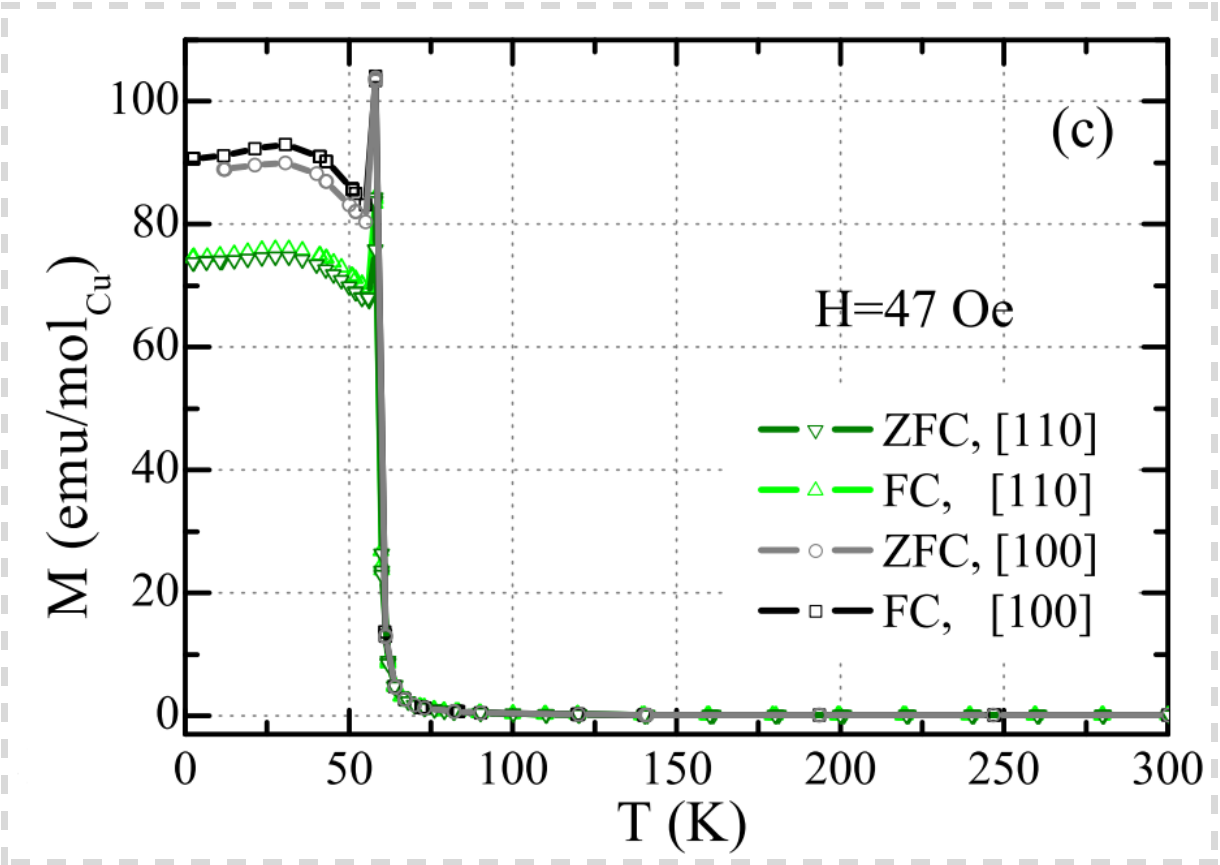

Figure 1.2a: The temperature dependence of the ZFC and FC magnetization of cubic Cu_2OSeO_3 measured in a magnetic field of 47 Oe applied along [110] and [100] direction. [23]

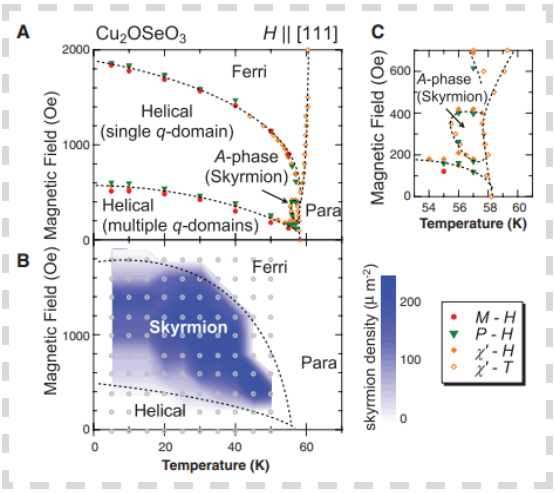

Figure 1.2b: Magnetic phase diagram under H || [111], deduced for (A) bulk and (B) thin-film forms of Cu_2OSeO_3, respectively. (C) Magnified view of (A) near the A-phase (skyrmion crystal phase) region. [3]

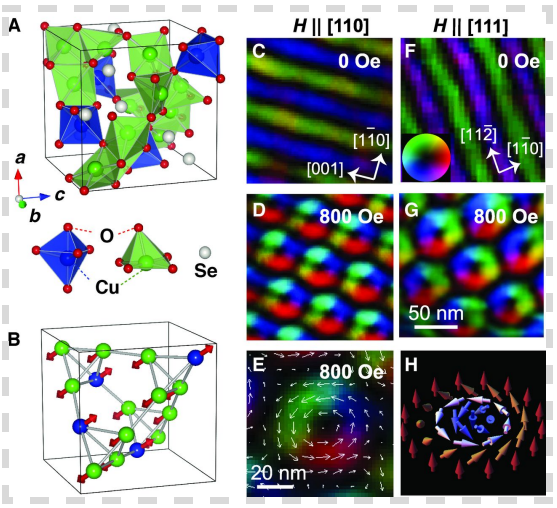

Figure 1.2c: (A) Crystal structure of Cu_2OSeO_3, characterized by two inequivalent Cu^{2+} sites with different oxygen coordination. (B) Ferrimagnetic spin arrangement on Cu^{2+} sites. (C to G) Lateral magnetization distribution map for a thin-film (~100-nm-thick) sample of Cu_2OSeO_3. A magnified view of (D) is shown in (E), where white arrows represent the magnetization direction. (H) Schematic illustration of a single magnetic skyrmion. [3]

1.2.2 $Cu_4O(SeO_3)_3$

$Cu_4O(SeO_3)_3$ is closely related to Cu_2OSeO_3 as part of the $Cu_xO(SeO_3)_{x-1}$ family and has a reported monoclinic and triclinic structure [2].

The monoclinic polymorph is reported to have similar magnetic behavior to that of Cu_2OSeO_3; both are primarily antiferromagnetic with a comparable Néel temperature around T=60K. It does however show an additional magnetic transition at T=13K and it was reasoned that the ground state is likely a helical antiferromagnet with a small ferromagnetic component, see *Figure 1.2d* [24].

No research on the magnetic or electrical properties of the triclinic polymorph has so far been published.

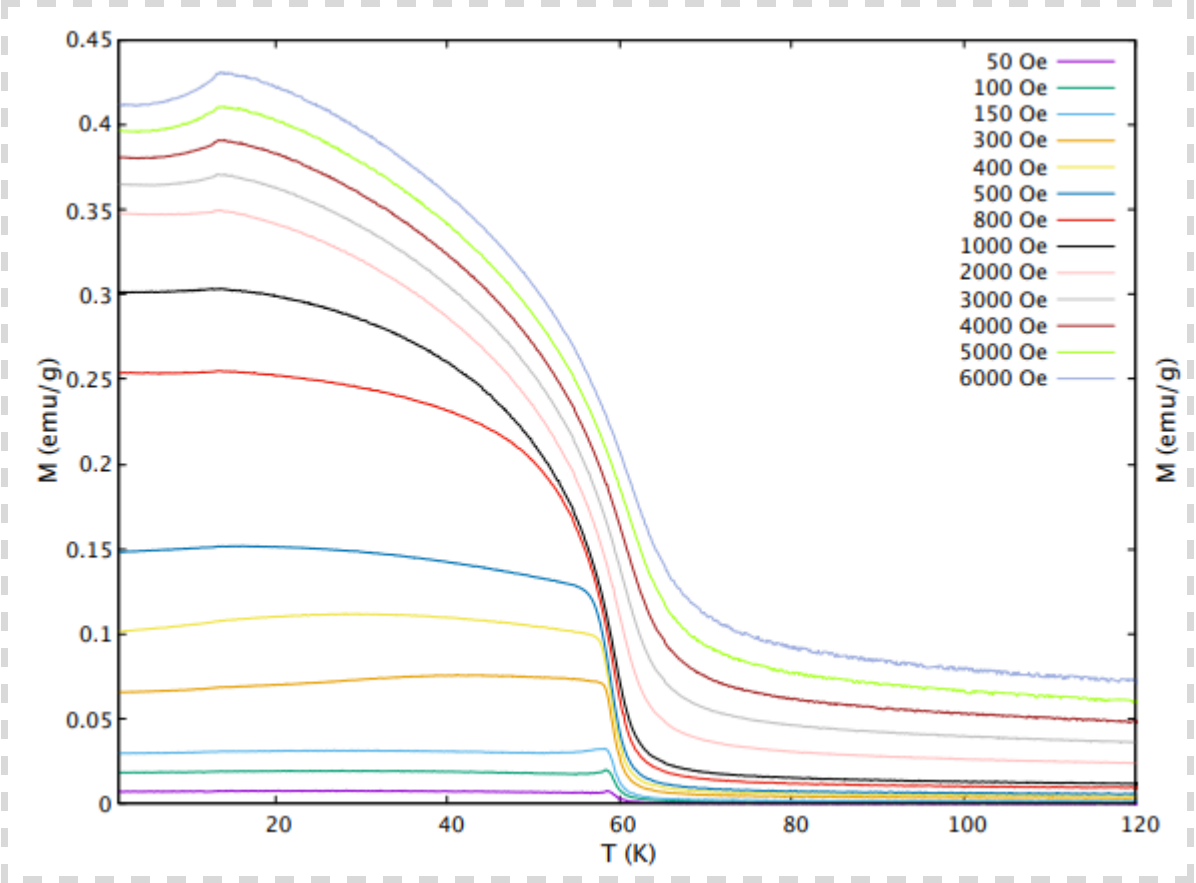

Figure 1.2d: Zero-Field Cooling (ZFC) M(T) curves for a single crystal of Cu4O(SeO3)3 for a set of applied magnetic fields [24].

1.2.3 $CuSeO_3$

$CuSeO_3$ is reported to have four polymorphs: one monoclinic, one triclinic, and two different orthorhombic polymorphs [15][16].

Structural and magnetic studies from 2012 on the monoclinic polymorph were carried out to investigate localized clusters of spins. The temperature dependency of the magnetic susceptibility features a broad maximum around T=18K and a Néel temperature around T=8K, based on heat capacity measurements [25].

More recently in 2020 the magnetic properties of the triclinic polymorph were reported. The temperature dependence and field dependence of the magnetic moment were shown up to 20K and a magnetic phase diagram was constructed, containing a paramagnetic phase, an induced ferromagnetic phase, and two helimagnetic phases with an insulating band gap of 3.90eV calculated from UV–Vis diffuse reflectance spectroscopy data. Theoretical calculations predicted a high degree of magnetic frustration which makes the triclinic phase a promising candidate for hosting magnetic skyrmions [26].

One of the reported orthorhombic polymorphs was studied for its magnetic properties. A ferromagnetic ordering was found with a Curie temperature of T=26K. The magnetization was measured to be 24.1 emu/g and remained unsaturated at T=4.2K and an applied field of 0.96T [15].

1.2.4 $CuSeO_3 \cdot 2H_2O$

$CuSeO_3 \cdot 2H_2O$ is also known as chalcomenite, a naturally occurring mineral. It forms as a light blue prism shaped crystal and has been reported to have an orthorhombic structure [1].

Its magnetic properties were studied most in depth in 2009. The temperature dependence of the magnetic moment was measured from T=5K to T=300K in an applied field of 0.1T and a primarily antiferromagnetic ordering was found below 30K with a weak ferromagnetic component [27].

1.2.5 $Cu_5O_2(SeO_3)_2Cl_2$

$Cu_5O_2(SeO_3)_2Cl_2$ has a reported α [17] and β [18] structure. The α structure, also known as georgbokiite, was analyzed and reported to consist of alternating layers of $Cu_2O_4Cl_2$ and Cu_3O_5Cl octahedra in the a-c plane, which were linked along the b-axis. The temperature dependence of the magnetic susceptibility was measured and showed a broad bump around T=97K argued to be characteristic of short range magnetic ordering, and a kink around T=32K indicating the onset of long range antiferromagnetic ordering.

The β structure, also known as parageorgbokiite, was analyzed and compared to that of georgbokiite. Both structures feature a common unit, denoted as {[O2Cu5](SeO3)2}2+ rods consisting of oxygen centered tetrahedra with selenite groups, with a difference in their ordering. In georgbokiite they form sheets in the a-c plane with linkages along the b-axis, whereas in parageorgbokiite they form a three dimensional network.

1.2.6 $Cu_9O_2(SeO_3)_4Cl_6$

$Cu_9O_2(SeO_3)_4Cl_6$ was found to have a long range antiferromagnetic ordering based on magnetization, specific heat, and neutron scattering measurements with a Néel temperature of T=37K. Temperature dependent x-ray diffraction and dielectric measurements also indicate an antiferroelectric order below T=267K with an anomaly showing signs of spin-lattice interactions [21].

1.3 Hydrothermal Synthesis

Many of the compounds studied in this thesis were prepared using hydrothermal synthesis [28]. A hydrothermal synthesis involves a sealed teflon insert placed in an

outer steel container container, called an autoclave. The teflon insert is filled with a water solution that is raised to a specific temperature and consequently a specific pressure. When the temperature is below the critical temperature of water the pressure is roughly equal to the vapor pressure of water at that temperature. This high-temperature, high-pressure environment causes the reagents to dissolve and react.

The crystallization of the products relies on the solution becoming supersaturated, which can be achieved by three different methods. The first of these is to introduce a temperature gradient in the solution, by which the reagents will dissolve and react on the hot end, saturating the solution, and be carried by convection currents to the cooler end where the solution will become supersaturated and the product will crystalize out of solution. Alternatively supersaturation can be achieved by slowly cooling the solution down at the end of the synthesis, which is a simpler method but provides less control. A third method relies on the difference in solubility of the reagents and products, since this method can only rarely be controlled it is usually combined with one of the first two methods.

1.4 Chemical Vapor Transport Synthesis

For the growth of larger crystals chemical vapor transport synthesis was used. Chemical vapor transport [29] is similar in concept to chemical vapor deposition, during which materials react at one end of a tube, either sealed or open ended, and become volatile after which they are carried by heat convection currents to deposit as crystals on the other end. However in the case of chemical vapor transport the desired product does not become volatile under the used reaction conditions. Instead a volatile material known as the transport agent has to be introduced to react with the product. This creates an intermediate product that is volatile, is able to be carried by the convection currents, and can deposit as crystals on the other end of the tube. Before crystallization, it is necessary that the intermediate phase decomposes back into the desired product and the transport agent, such that crystals of the desired product are obtained. The transport agent thus acts as a catalyst and when a sealed container is used the agent is able to go back and forward, repeatedly aiding the growth of crystals during the reaction.

The direction of this transportation is based on the thermodynamics of the reaction between the reagents and the transport agent. For an exothermic reaction the product should react with the transport agent at the cooler end and be deposited at the hotter end, where the equilibrium of the reaction will be less favorable. An endothermic reaction should instead be designed to react at the hotter end and deposit at the cooler end. The temperature gradient, the type and amount of the transport agent, and the dimensions of the tube are all variables that can be optimized according to the thermodynamics and free energy of the desired reaction.

1.5 X-ray Crystallography

Determining the structure of a crystal is essential for building a better understanding of its material properties. A common and accurate method is x-ray crystallography, which relies on the specific symmetry of the crystal lattice producing a specific diffraction pattern. These diffraction patterns can be understood by considering interference of the diffracted x-ray beams. Incoming x-ray waves are diffracted by different scatterers, producing multiple outgoing spherical waves that will interfere with each other. When considering the multitude of scatterers in a crystal the outgoing waves will generally destructively interfere, except when the difference in the path length of the outgoing waves is such that through the symmetry of the scatterers they line up and constructively interfere. This relationship is described by Bragg's law: $n\lambda = 2d \sin\theta$. Where n is any (positive) integer, λ is the wavelength of the x-ray waves, d is the distance between parallel planes of the periodically arranged scatterers, and θ is the angle of the incoming x-ray beam to the particular set of lattice planes.

For single crystals the diffraction pattern on a two dimensional detector is an array of dots while for a powder the crystals are generally considered to be uniformly distributed across all possible orientations causing the diffraction pattern as captured by a two dimensional detector to become a series of concentric rings with different spacings related to 2θ. Generally powder x-ray diffraction patterns are shown as a plot of the intensity versus 2θ, effectively taking a one-dimensional cut through the aforementioned rings.

1.6 SQUID Magnetometry

Determining the magnetic response of a sample is generally quite simple. The sample is put in a temperature controlled environment in which a magnetic field can be applied. The magnetic response of the sample can then be measured by moving it up and down through a conducting coil which will generate Eddy currents in response to the changing magnetic field from the moving sample, as per Faraday's law of induction.

The importance of SQUID (superconducting quantum interference device) magnetometers lies in their unparalleled sensitivity [30]. This is achieved by using a quantum phenomena known as the Josephson effect to measure the magnetic response instead of a simple conducting coil. The Josephson effect occurs in junctions of two superconductors separated by a thin insulating barrier, where electron pairs known as Cooper pairs, described in the Bardeen-Cooper-Schrieffer theory on superconductors, are able to tunnel through the thin barrier and generate a small spontaneous current. The chance of this tunneling and consequently the amplitude of the generated current is highly sensitive to the local magnetic field and can thus be used to measure very small changes in the magnetic field caused by a magnetic sample being moved across the junction.

1.7 Previous Work

The syntheses procedures employed in this thesis have been partially optimized by previous bachelor students and members of the research group at the University of Groningen led by Dr. G.R. Blake.

Eugene Gvozdetsky investigated the use of the more water soluble $Cu(OH)_2$ instead of the previously used CuO for the hydrothermal synthesis. Three different chemical vapor transport syntheses with HCl, $SeCl_4$, or $TeCl_4$ as the transport agent were also performed.

Both Sanne Berg and Winfried de Haas continued this work not long afterwards, focusing on optimizing the hydrothermal synthesis method by varying the temperature, reaction times, and water fill percentage in the teflon insert.

2 Methods

Experiment #	Synthesis	Reagents
1	Hydrothermal	1:1 molar ratio of $Cu(OH)_2$ and SeO_2
2	Hydrothermal	4:3 molar ratio of $Cu(OH)_2$ and SeO_2
3	Chemical Vapor Transport	4:3 molar ratio of CuO and SeO_2
4	Hydrothermal	3:2 molar ratio of $Cu(OH)_2$ and SeO_2
5	Hydrothermal	2:1 molar ratio of $Cu(OH)_2$ and SeO_2
6	Chemical Vapor Transport	2:1 molar ratio of CuO and SeO_2
7	Chemical Vapor Transport	4:3 molar ratio of CuO and SeO_2

Table 2a: An overview of the performed syntheses, numbered chronologically.

2.1 Hydrothermal Synthesis

The appropriate molar ratio of material was weighed, see *Table 2.1a*, and transferred to a 50ml teflon autoclave insert, to which 40ml demi-water was added to fill the insert to 80%. This yields a pressure of approximately 10 bar at the synthesis temperature of 180℃, the vapor pressure of water at that temperature.

Experiment #	$Cu(OH)_2$ (g)	SeO_2 (g)	Molar Ratio
1	5.71	6.65	1 : 1.02
2	6.62	5.63	4 : 2.99
4	6.67	5.43	3 : 2.11
5	3.90	2.22	2 : 1.00

Table 2.1a: The weighed amounts of starting material used in the hydrothermal syntheses.

A magnetic stirring egg and hot plate set to 70℃ were used to dissolve and mix the starting materials as much as possible for 20 minutes. After retrieving the magnetic stirring egg the teflon insert was transferred to a steel autoclave and tightly closed. The autoclave was placed in a box furnace and heated according to the schedule shown in *Figure 2.1a*. Supersaturation and the resulting crystal formation is driven by the natural slow cooling after holding at 180℃ for 72 hours.

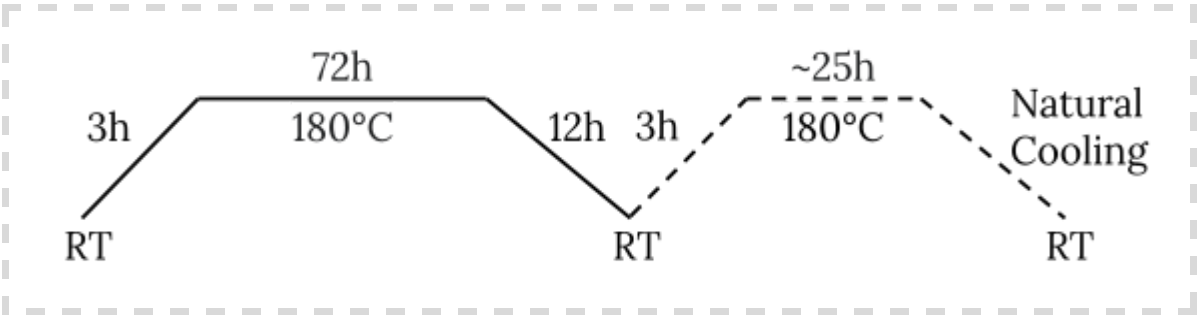

Figure 2.1a: The heating schedule used for the hydrothermal syntheses. The second heating cycle was only applied to sample 4.

After the heating cycle the autoclave was opened and the crystals were harvested, which were either floating on the surface of the water, attached to the sides of the teflon insert or piled up at the bottom. The crystals were washed with demi-water to dissolve any leftover starting materials and dried in a furnace for 1.5 hours at 70℃.

2.2 Chemical Vapor Transport Synthesis

The materials were weighed, see *Table 2.2a*, in a nitrogen atmosphere inside a glove box and mixed together using a mortar and pestle before being transferred to the bottom of a 30cm quartz tube. The tube was then evacuated and flame sealed before being placed across two zones of a three-zone tube furnace with separate heating elements to perform the desired heating schedule as shown in *Figure 2.2a*.

Experiment #	CuO (g)	SeO_2 (g)	$SeCl_4$ (g)	Molar Ratio (CuO:SeO_2)
3	3.13	3.21	0.62	4:2.95
6	2.84	1.96	0.50	2:0.99
7	2.44	2.52	0.24	4:2.96

Table 2.2a: The weighed amounts of starting material used in the chemical vapor transport syntheses.

After the tube was allowed to cool down naturally it was carefully broken open to retrieve the crystals.

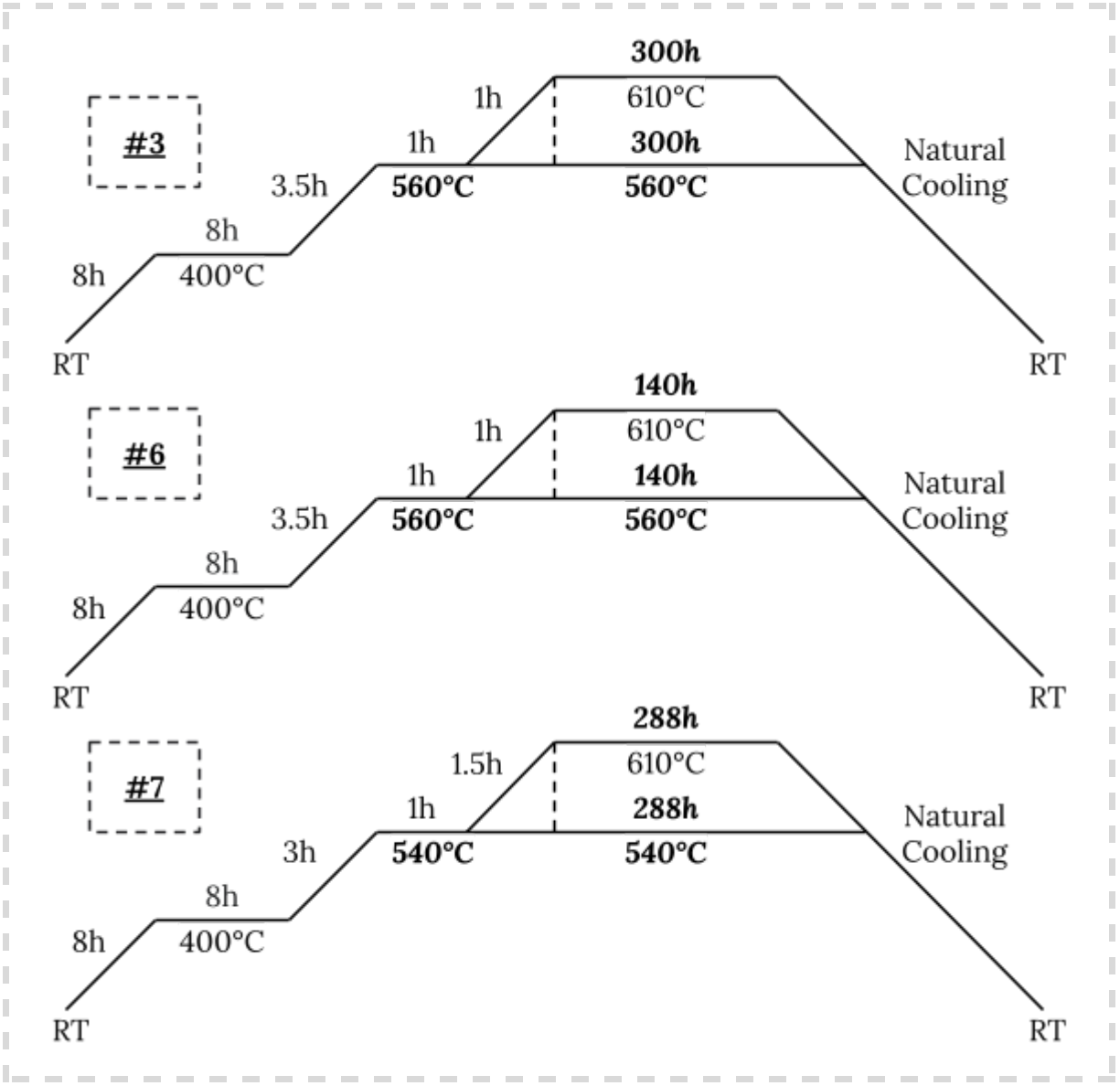

Figure 2.2a: The heating schedule used for the chemical vapor transport syntheses.

2.3 Single Crystal X-ray Diffraction

All crystals that could be differentiated by eye and could be found in high enough quality had their structure identified by single crystal x-ray diffraction.

These measurements were performed on a Bruker D8 Venture diffractometer at room temperature using copper and molybdenum x-ray sources with wavelengths of 1.54 and 0.71 Å respectively. Fast scans were performed to estimate the lattice parameters and identify each crystal by comparing with previous literature reports. To determine the full crystal structures, refinements were performed using data sets consisting of several hundred or thousand data frames.

The resulting structures were visualized using VESTA [31].

2.4 Powder X-ray Diffraction

Powder x-ray diffraction was used to confirm the compounds present in the samples. It was not used for detailed structural analysis.

These measurements were performed on a Bruker D8 Advance diffractometer at room temperature using a copper x-ray source. Short scans were performed to confirm the quality of the sample, after which full scans of 2θ ranging from 10° to 90° were taken. Rietveld refinements were performed on the data using the relevant structural phases that were obtained from single crystal x-ray diffraction of the produced samples or from previous literature.

2.5 Magnetic Measurements

DC Temperature and field dependency measurements of the magnetic moment were performed on an MPMS (magnetic property measurement system) equipped with a SQUID (superconducting quantum interference device).

3 Results & Discussion

Reaction	Experiment #	Identified Products
HT	1 (1:1)	$CuSeO_3$ (m), $CuSeO_3 \cdot 2H_2O$
	2 (4:3)	$CuSeO_3$ (m), $CuSeO_3 \cdot 2H_2O$, Cu_2OSeO_3 (c), $Cu_4O(SeO_3)_3$ (t)
	4 (3:2)	$CuSeO_3$ (m), $CuSeO_3 \cdot 2H_2O$, Cu_2OSeO_3 (c), $Cu_4O(SeO_3)_3$ (m), $Cu_4O(SeO_3)_3$ (t)
	5 (2:1)	$CuSeO_3$ (m), Cu_2O, $CuSeO_3 \cdot 2H_2O$, Cu_2OSeO_3 (c)
CVT	3 (4:3)	$CuSeO_3$ (t), $Cu_5O_2(SeO_3)_2Cl_2$, $Cu_9O_2(SeO_3)_4Cl_6$
	6 (2:1)	$CuSeO_3$ (t), $Cu_5O_2(SeO_3)_2Cl_2$, $Cu_9O_2(SeO_3)_4Cl_6$
	7 (4:3)	$CuSeO_3$ (t), $Cu_4O(SeO_3)_3$ (m), $Cu_5O_2(SeO_3)_2Cl_2$

Table 3a: The identified products from each experiment.

Identified Product	Experiment #s
$CuSeO_3$ (m)	1, 2, 4, 5
$CuSeO_3$ (t)	3, 6, 7
$CuSeO_3 \cdot 2H_2O$	1, 2, 4, 5
Cu_2OSeO_3 (c)	2, 4, 5
$Cu_4O(SeO_3)_3$ (m)	4, 7
$Cu_4O(SeO_3)_3$ (t)	2
$Cu_5O_2(SeO_3)_2Cl_2$	3, 6, 7
$Cu_9O_2(SeO_3)_4Cl_6$	3, 6

Table 3b: The experiment numbers each identified relevant product was found in.

	a [Å]	b [Å]	c [Å]	α [°]	β [°]	γ [°]	V [Å³]	ρ [g/cm³]	Space Group
$CuSeO_3$ III	7.7184(3)	8.2413(3)	8.5010(3)	-	99.147(3)	-	533.87(3)	4.740	$P2_1/n$
$CuSeO_3$ IV	4.7330(1)	8.5748(3)	10.6152(3)	66.651(1)	88.525(1)	88.383(1)	395.33(2)	4.801	$P\bar{1}$
$CuSeO_3 \cdot 2H_2O$	6.6704(12)	7.3831(13)	9.1582(16)	-	-	-	451.03(14)	3.336	$P2_12_12_1$
Cu_2OSeO_3 I	8.9264(2)	-	-	-	-	-	711.26(5)	2.522	$P2_13$
$Cu_4O(SeO_3)_3$ I	15.9720(13)	13.4836(14)	17.6800(18)	-	90.626(3)	-	3807.33(99)		$P2_1/a$
$Cu_4O(SeO_3)_3$ II	7.9920(2)	8.1446(3)	8.3959(3)	77.353(2)	65.561(2)	81.317(2)	484.34(3)	4.464	$P\bar{1}$
$Cu_5O_2(SeO_3)_2Cl_2$ I	6.0451(2)	13.7871(6)	5.5778(2)	-	95.768(2)	-	462.52(3)	4.843	$P2_1/c$
$Cu_9O_2(SeO_3)_4Cl_6$ II	12.9384(7)	6.2715(4)	14.0553(8)	-	112.847(2)	-	1051.01(11)	4.185	$P2_1/n$

Table 3c: Structural data of crystals identified by single crystal x-ray diffraction.

3.1 Hydrothermal Synthesis

All the hydrothermal syntheses provided a good yield of crystals with almost no starting materials left unreacted. The quality of crystals varied widely however. For an overview of the various crystals identified in each experiment, *Table 3a* and *Table 3b* can be consulted. The room temperature lattice parameters of all crystals identified by single crystals x-ray diffraction can be found in *Table 3c*.

3.1.1 Experiment 1 - 1:1 molar ratio

Experiment 1 with a 1:1 molar ratio of the starting materials $Cu(OH)_2$ and SeO_2 yielded almost exclusively crystals in the form of light-green sheets and spheres, and a few light-blue prisms. The majority of the light-green crystals were stuck together in bulbous polycrystalline formations but single crystals of high enough quality could still be found for analysis. All of the light-blue crystals appeared to be single crystals and were noticeably larger.

A picture taken of the product through an optical microscope is shown in *Figure 3.1a*.

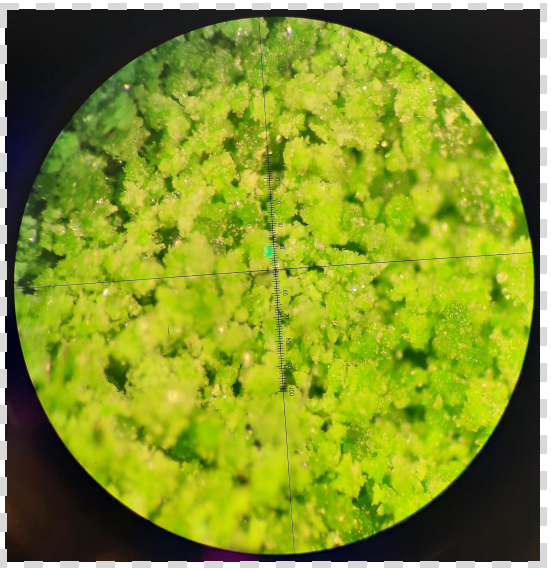

Figure 3.1a: Product obtained from Experiment 1. The picture was taken through an optical microscope but the exact scale is unknown.

3.1.1.1 Single Crystal X-ray diffraction

The light-green crystals were identified as the monoclinic polymorph of $CuSeO_3$ with the $P2_1/n$ space group, which is in agreement with previous literature reports [16]. The refined structure is shown in *Figure 3.1b*. All the copper cations are bonded to 5 oxygen anions in a distorted square pyramidal formation and all the selenium atoms are 3-coordinated in triangular pyramidal geometry in the form of selenite (SeO_3^{2-}) anions. The structure contains multiple loops of edge and corner-shared polyhedra consisting of both copper-oxygen-copper and copper-oxygen-selenium linkages.

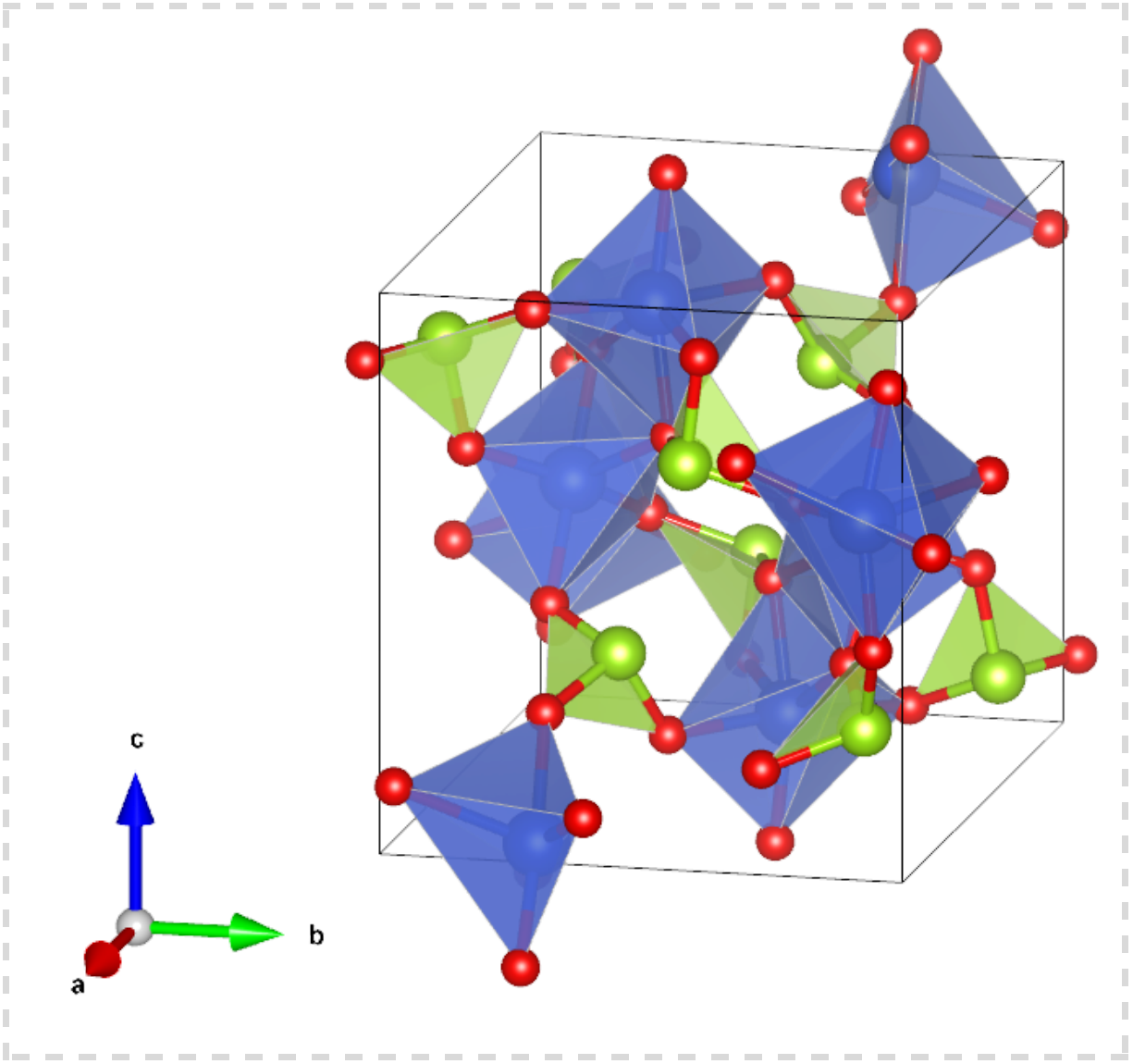

Figure 3.1b: Refined crystal structure of monoclinic $CuSeO_3$.

The light-blue crystals were identified as the orthorhombic $CuSeO_3 \cdot 2H_2O$ with the $P2_12_12_1$ space group, in agreement with previous literature reports [1]. The refined structure is shown in *Figure 3.1c*. The copper cations are bonded to 5 oxygen anions in a distorted square pyramidal formation and all the selenium cations are in the form of SeO_3^{2-} anions. No copper-oxygen-copper linkages are present in this structure; the

copper cations are all linked through copper-oxygen-selenium-oxygen-copper linkages instead. This results in a rather disperse pattern of CuO_5 polyhedra that are partially connected by hydrogen bonding through the water molecules.

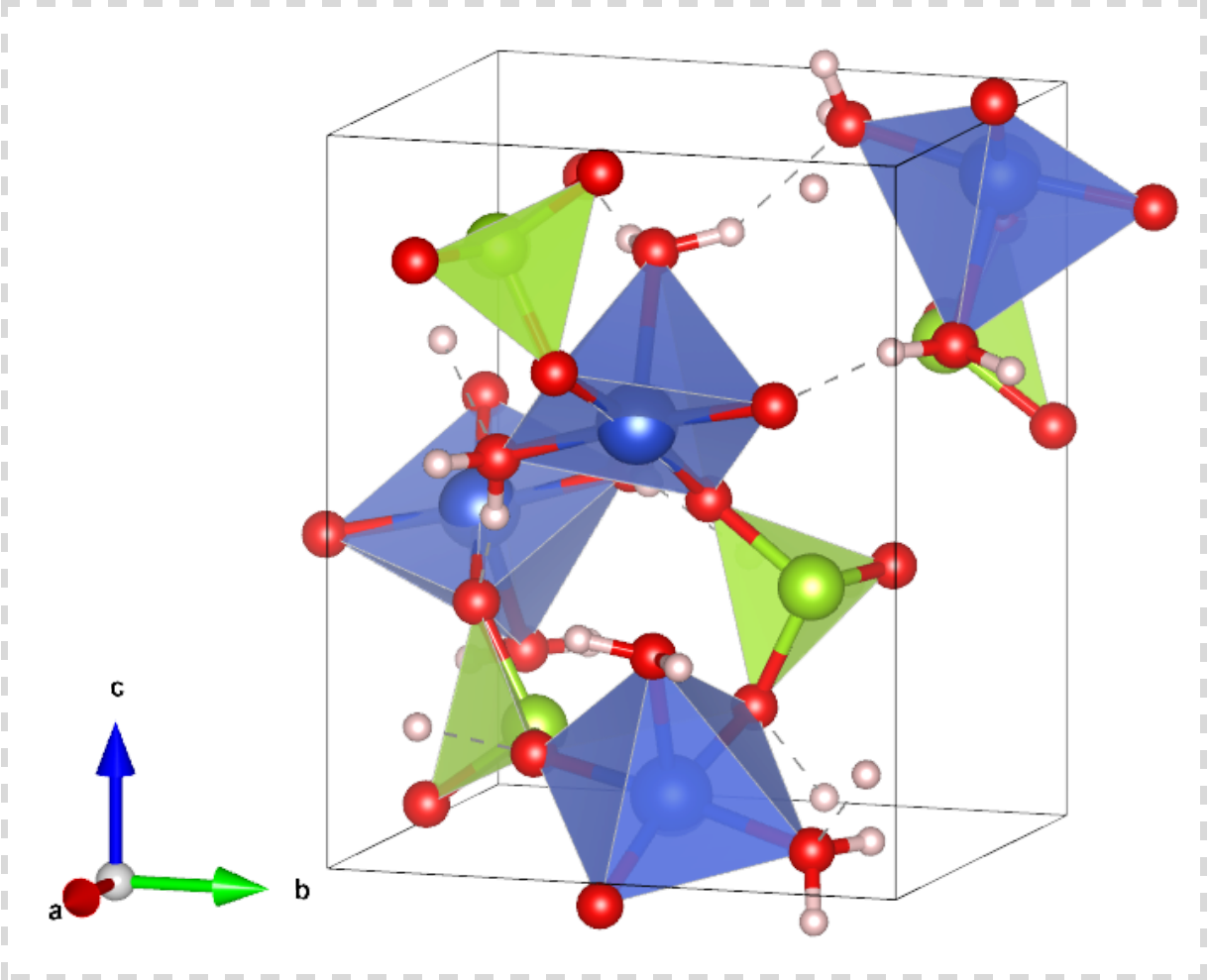

Figure 3.1c: Refined crystal structure of orthorhombic $CuSeO_3 \cdot 2H_2O$.

3.1.1.2 Powder X-ray diffraction

Figure 3.1d shows the powder x-ray diffraction pattern of the green product from *Experiment* 1 fitted using the monoclinic $CuSeO_3$ structure obtained from single crystal x-ray diffraction of *Experiment* 1. All peaks are accounted for and a final wRp value of 7.59% was obtained.

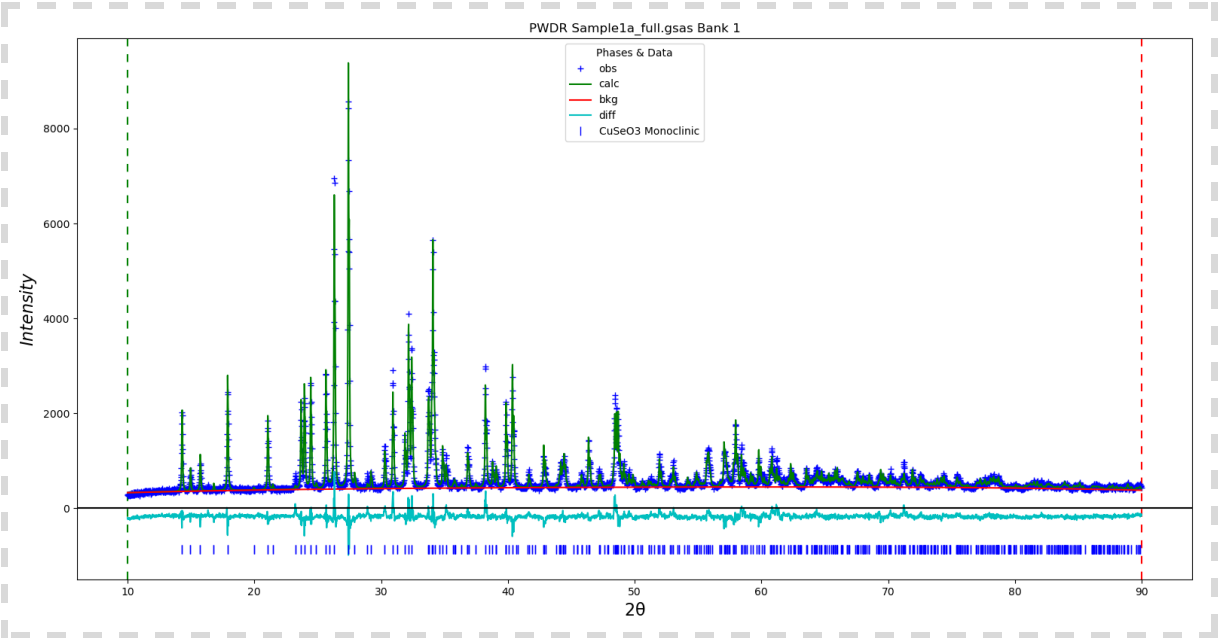

Figure 3.1d: Fitted powder x-ray diffraction pattern of the green product from Experiment 1.

3.1.2 Experiment 2 - 4:3 molar ratio

Experiment 2 with a 4:3 Cu:Se molar ratio also yielded light-green and light-blue crystals, but dark-green sheets and golden-brown rods were also present in roughly equal amounts to the light-green crystals. The dark-green crystals were often stuck together in polycrystalline bulbous formations of similar sizes. The golden-brown rods could also be found stuck together, pointing out from a common base in radial fashion, but plenty of single crystals were present for analysis.

A picture taken of the product through an optical microscope is shown in Figure 3.1e.

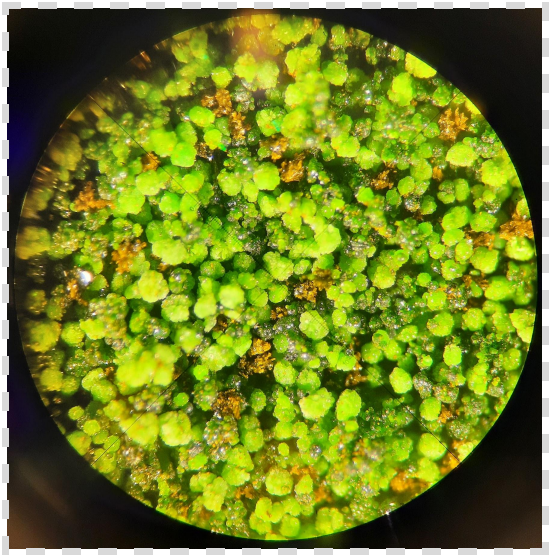

Figure 3.1e: Product obtained from Experiment 2. The picture was taken through an optical microscope but the exact scale is unknown.

3.1.2.1 Single Crystal X-ray diffraction

The light-green crystals were identified as the monoclinic polymorph of $CuSeO_3$. The structure was refined using crystals from *Experiment* 1 and is shown in *Figure 3.1b*.

The light-blue crystals were identified as orthorhombic $CuSeO_3 \cdot 2H_2O$. The structure was refined using crystals from *Experiment* 1 and is shown in *Figure 3.1c*.

The golden-brown crystals were identified as the triclinic polymorph of $Cu_4O(SeO_3)_3$ with the $P\bar{1}$ space group, which is in agreement with previous literature reports [2]. The refined structure is shown in *Figure 3.1f*.

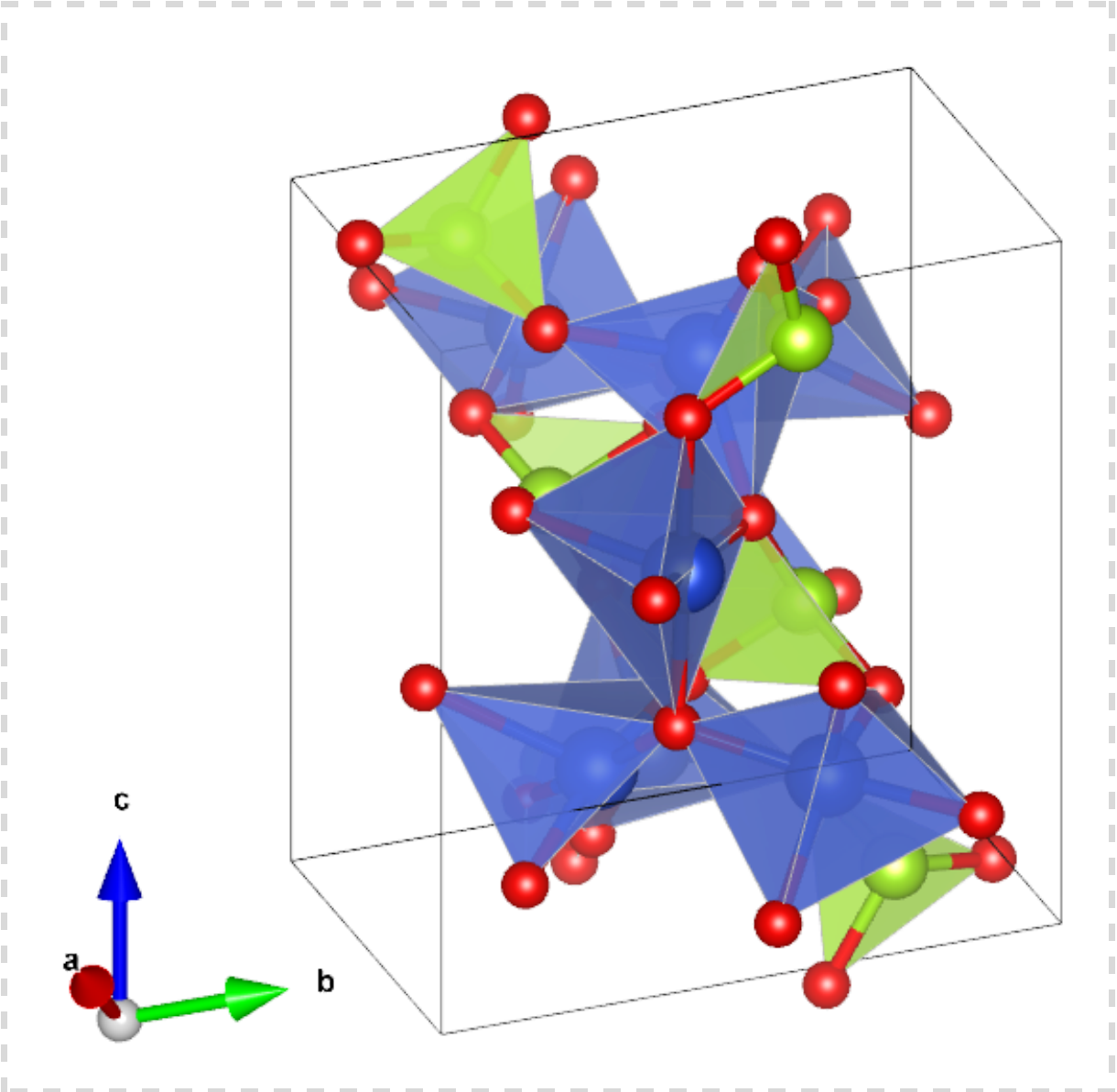

Figure 3.1f: Refined crystal structure of triclinic $Cu_4O(SeO_3)_3$.

All the copper cations are bonded to 5 oxygens in a distorted square pyramidal configuration and all the selenium cations are in the form of SeO_3^{2-} anions. The distortions of the square pyramidal configurations of CuO_5 are quite distinct, see Figure 3.1g and 3.1h. For half of the Cu^{2+} cations, one of the three oxygen atoms in the basal plane of the pyramid is shifted below the plane towards a trigonal bipyramidal configuration. These different configurations are reminiscent of cubic Cu_2OSeO_3, which features four trigonal bipyramidal coordinations and twelve square pyramidal configurations per unit cell, which is argued to lead to antiparallel alignment of the spins and ferrimagnetic ordering (see Figure 1.2c).

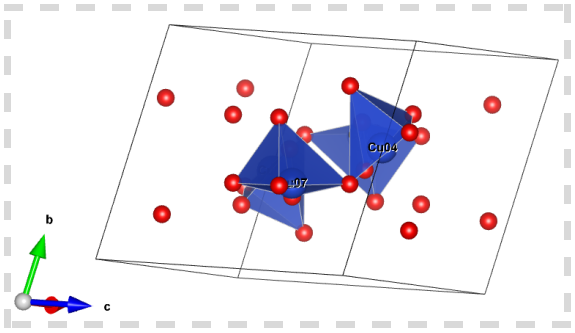

Figure 3.1g: Least distorted square pyramidal configurations of copper oxygen coordinations.

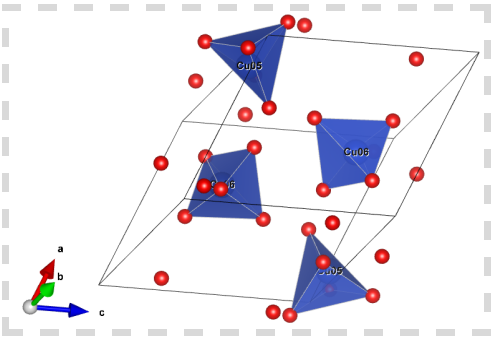

Figure 3.1h: Most distorted square pyramidal configurations of copper oxygen coordinations

The triclinic $Cu_4O(SeO_3)_3$ structure also exhibits some similarities to its monoclinic counterpart when looking at multiple unit cells, see Figure 3.1i and 3.1j. Both feature sheets with copper-oxygen-copper interlinkages forming channels through the material. The spacing in the triclinic structure is noticeably bigger and the structure features less copper-oxygen-copper interlinkages between the sheets, causing larger channels.

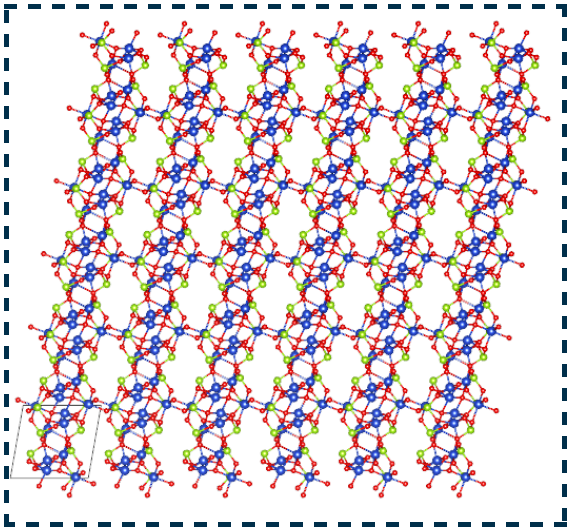

Figure 3.1i: Triclinic $Cu_4O(SeO_3)$ viewed along the b-c plane.

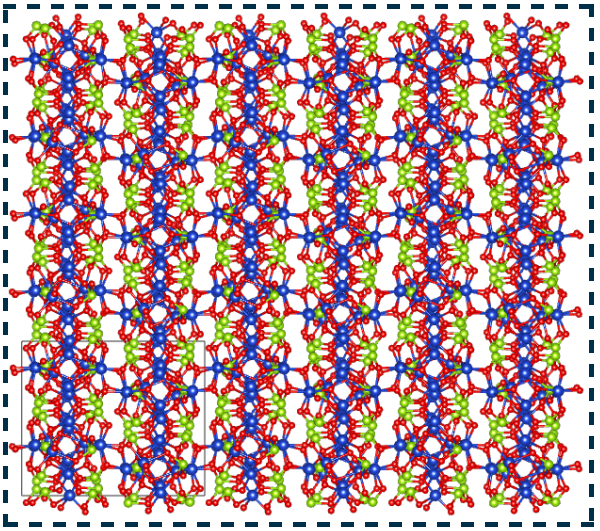

Figure 3.1j: Monoclinic $Cu_4O(SeO_3)$ viewed along the a-b plane. [2]

The dark-green crystals were identified as the cubic polymorph of Cu_2OSeO_3 with the $P2_13$ space group, which is in agreement with previous literature reports [2]. The refined structure is shown in Figure 3.1k. All the copper cations are bonded to 5 oxygen anions; one distinct copper cation is coordinated in a distorted square pyramidal configuration while the other is coordinated in a more tetragonal bipyramidal fashion. All the selenium cations are in the form of SeO_3^{2-} anions.

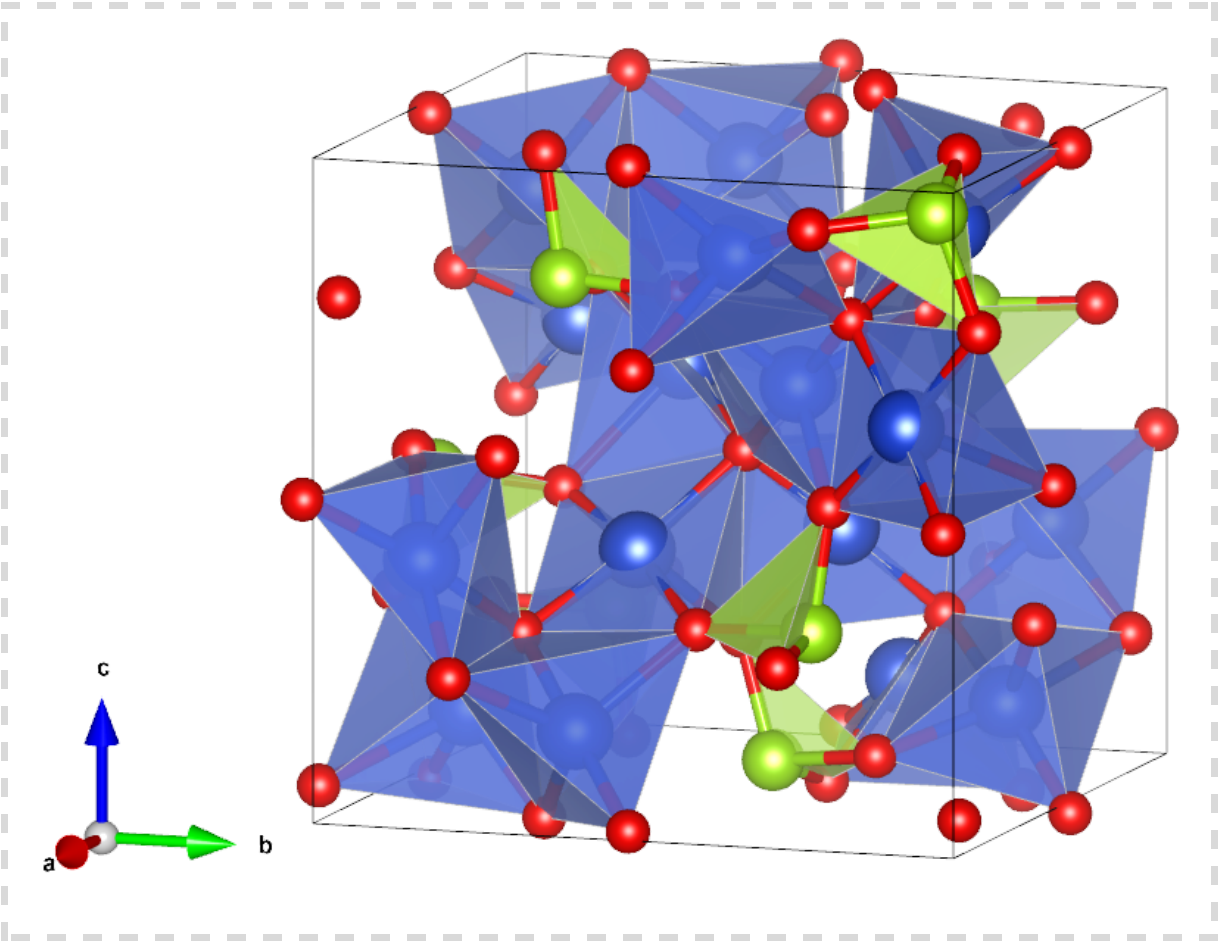

Figure 3.1k: Refined crystal structure of cubic Cu_2OSeO_3.

3.1.2.2 Magnetic Measurements

The temperature dependence of the magnetisation of triclinic $Cu_4O(SeO_3)_3$ was measured from 5K to 300K at an applied field of 0.5T, in field cooled and zero field cooled modes. These measurements are shown in Figure 3.1l. The field dependence of the magnetization was measured from -1T to 1T at temperatures of 10K, 30K, 50K, and 60K, shown in Figure 3.1n. A more in-depth measurement of the field and temperature dependence was also taken from 0T to 0.1T at temperatures ranging from 52K to 60K at 0.5K intervals, shown in Figure 3.1o. The derivative of these measurements was taken over five adjacent data points to look for any subtle changes in the trend, shown in Figure 3.1p. Individual crystals of triclinic $Cu_4O(SeO_3)_3$ were too small to give any signal in the SQUID magnetometer. Therefore approximately 500 individual crystals were

selected and stuck to a length of kapton tape with random orientations. Because the mass of this sample was still too small to measure reliably, the magnetization of the material could not be determined as an absolute value, but qualitative comparisons with literature reports of related materials can still be made. *Figure 1.2a* and *1.2d* display the magnetisation versus temperature of the cubic phase of Cu_2OSeO_3 [23] and the monoclinic phase of $Cu_4O(SeO_3)_3$ [24] respectively.

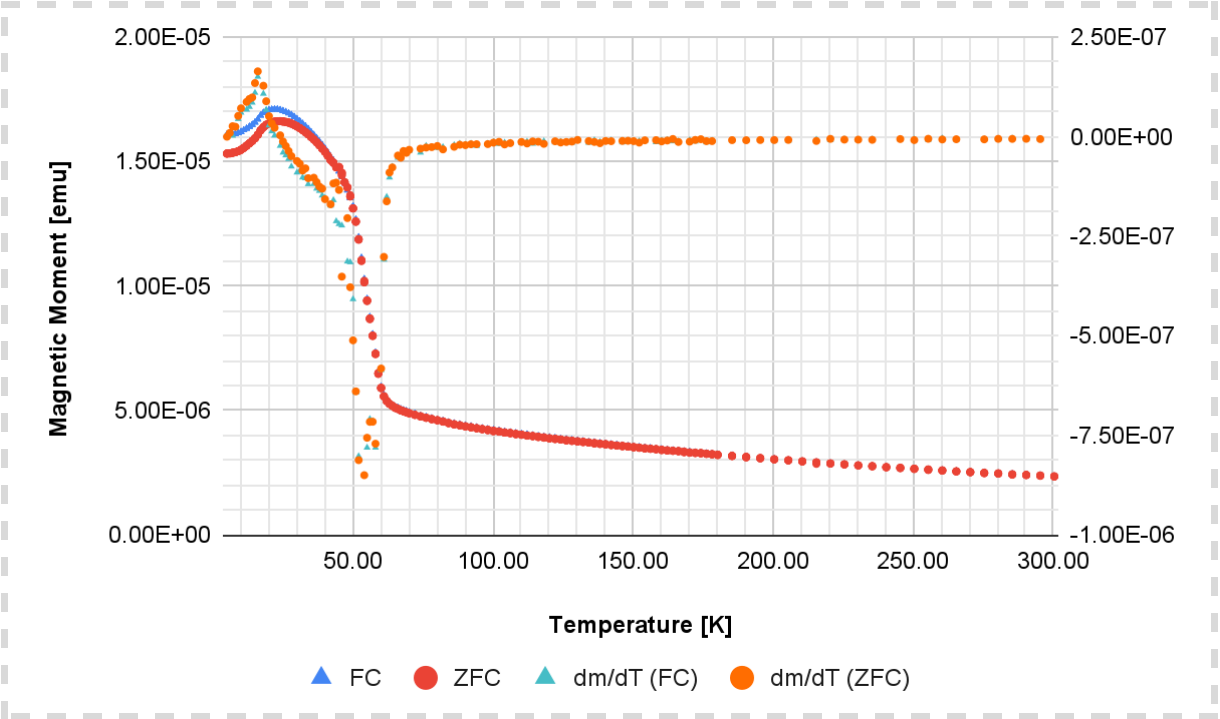

Figure 3.1l: The temperature dependence of the magnetization of triclinic $Cu_4O(SeO_3)_3$ (left) and its first derivative taken over three adjacent data points (right).

The temperature dependence of the magnetization of triclinic $Cu_4O(SeO_3)_3$, as seen in *Figure 3.1l*, suggests a primarily antiferromagnetic ordering with a Néel temperature of around T=63K. Based on the structural analysis of triclinic $Cu_4O(SeO_3)_3$, see section 3.1.2.1, and cubic Cu_2OSeO_3 [3][22][23], it is possible that spins associated with the four Cu^{2+} cations that have a coordination most distorted from square pyramidal towards a trigonal bipyramidal configuration are aligned antiparallel to spins associated with the four other Cu^{2+} cations that show a less distorted square pyramidal configuration. However, the rather sharp increase in magnetisation between 63K and 48K suggests the presence of a small net ferromagnetic component, which could arise either from a small degree of spin rotation away from an antiparallel configuration, or from ferrimagnetic ordering. Another possible magnetic phase transition is found at T=16K and is most noticeable in the derivative of the magnetic moment with respect to temperature. A comparable transition can be found for monoclinic $Cu_4O(SeO_3)_3$ at T=13K and it is suggested that a reorientation of the spins occurs [24]. Above T=63K the material transitions into a purely paramagnetic phase, based on the linear dependence of the inverse magnetisation on temperature (Curie-Weiss law), see *Figure 3.1m*.

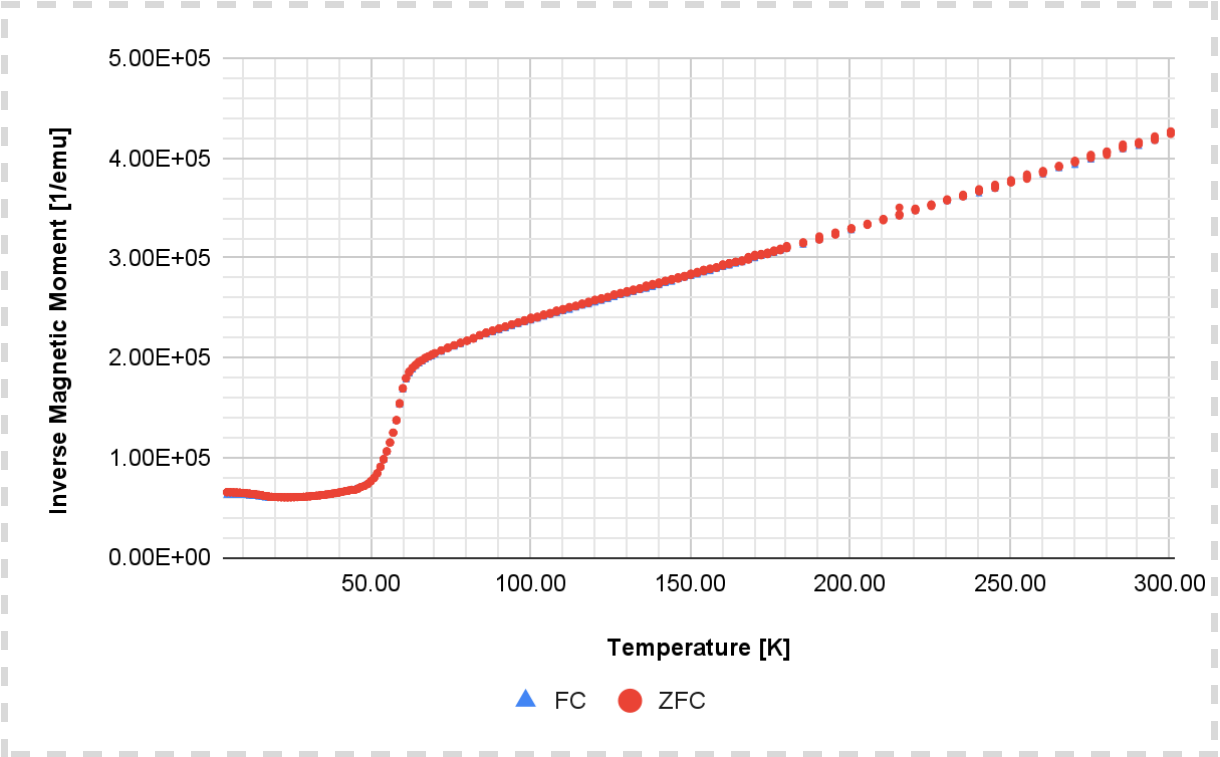

Figure 3.1m: The inverse of the magnetization of triclinic $Cu_4O(SeO_3)_3$, measured from 5K to 300K in a 0.5 T applied magnetic field.

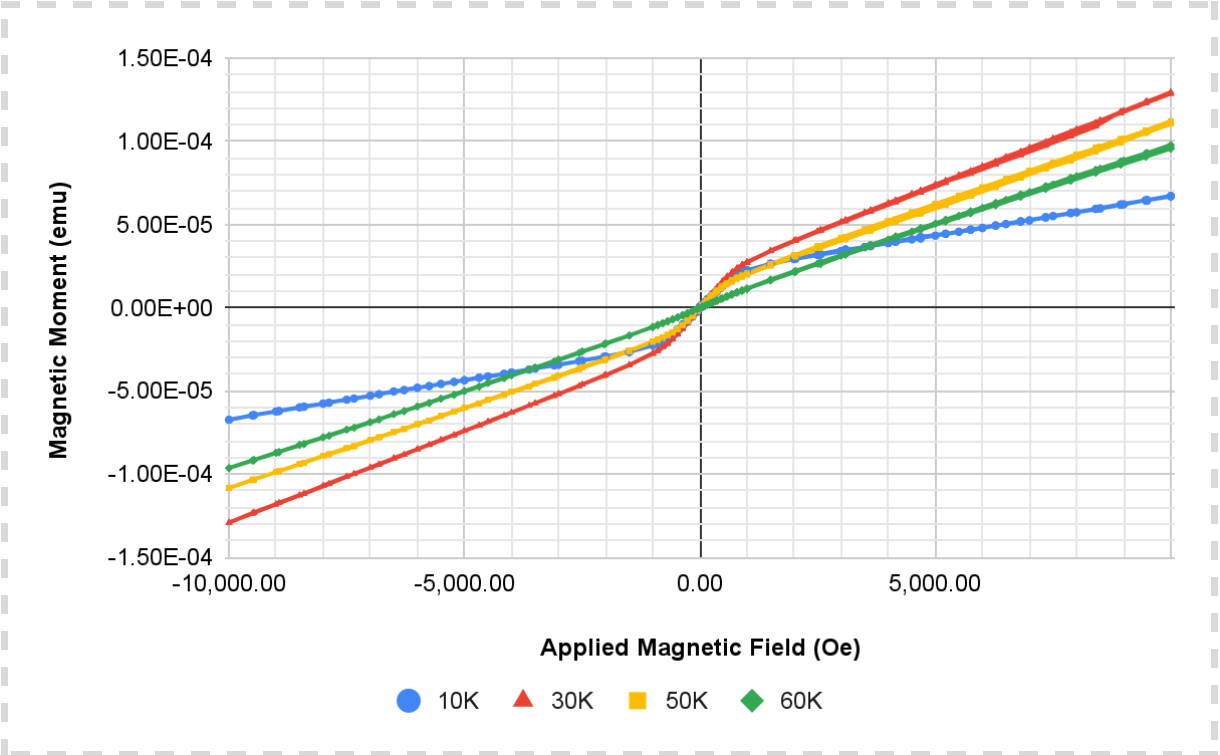

Figure 3.1n: The magnetization of triclinic $Cu_4O(SeO_3)_3$ measured at 10K, 30K, 50K, and 60K in applied magnetic fields ranging from -1T to +1T.

A clear indication of the skyrmion phase in cubic Cu_2OSeO_3 is an anomaly that is visible in the derivative of the magnetisation versus applied field measurements over a small temperature range near the PM-AFM transition. Magnetic skyrmions were not expected to be found in triclinic $Cu_4O(SeO_3)_3$ because of its centrosymmetry, but because of the otherwise similar structure to Cu_2OSeO_3 a detailed scan of the magnetisation versus applied field was performed over a field and temperature range similar to that where the skyrmion phase in bulk Cu_2OSeO_3 is found, see *Figure 3.1o*. The derivative, see *Figure 3.1p*, although noisy shows no signs of any anomaly that would indicate a transition to a skyrmion phase.

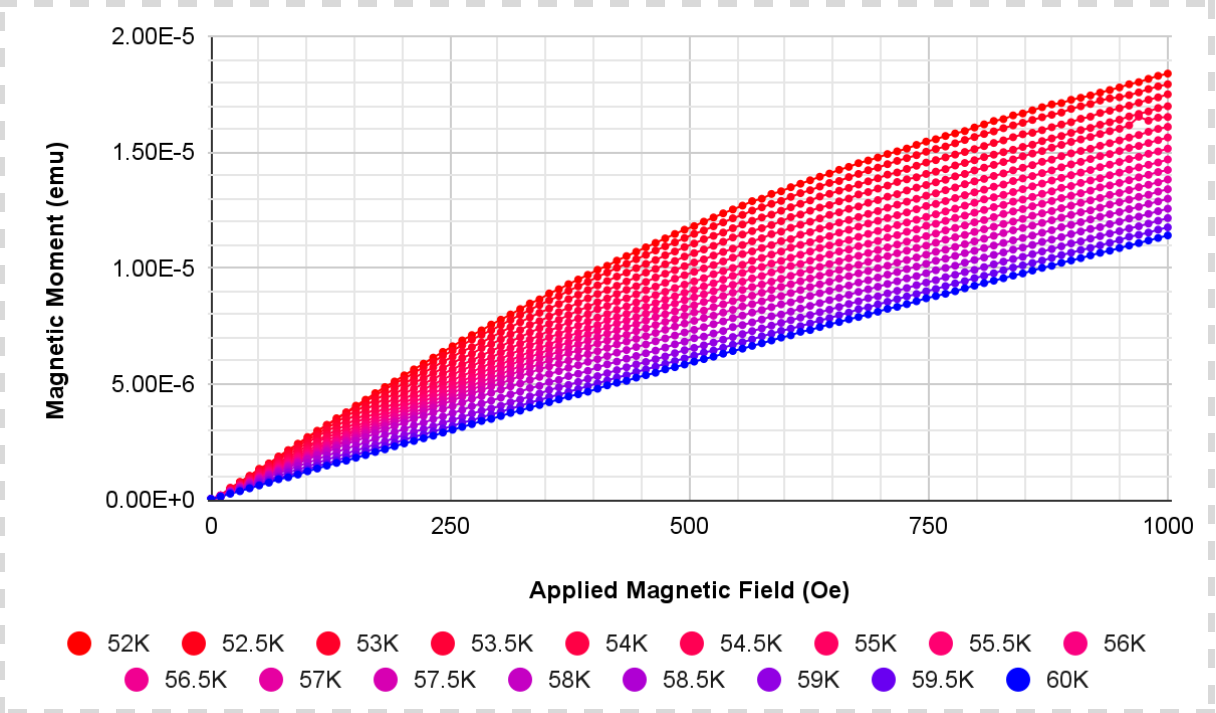

Figure 3.1o: The magnetization of triclinic $Cu_4O(SeO_3)_3$ measured at temperatures ranging from 52K to 60K at intervals of 0.5K in applied magnetic fields increased from 0T to +0.1T.

AC susceptibility measurements were attempted but no signal was obtained; such measurements would likely require an even higher sample mass. For these more in-depth measurements it is advised to optimize the hydrothermal synthesis for the growth of larger triclinic $Cu_4O(SeO_3)_3$ crystals, for example by using the small crystals obtained from the current hydrothermal synthesis as seed crystals.

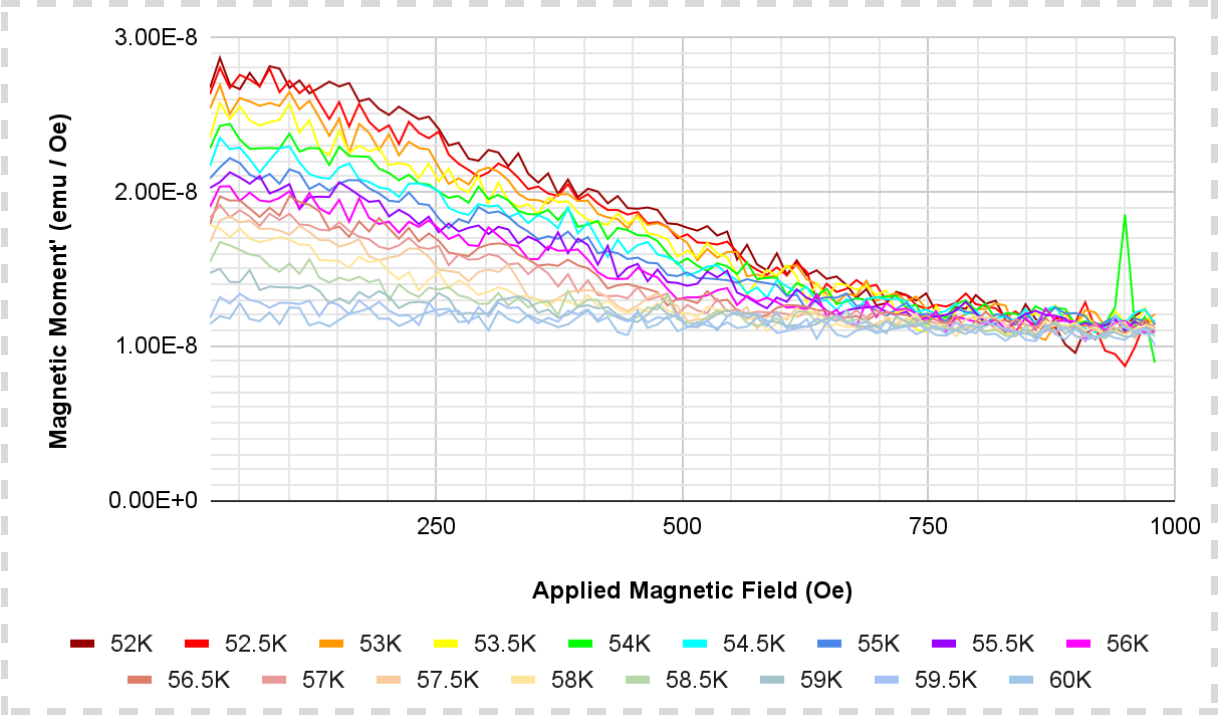

Figure 3.1p: The derivative of the magnetization versus the applied magnetic field, taken over five adjacent data points.

3.1.3 Experiment 4 - 3:2 molar ratio

Experiment 4 with a 3:2 molar ratio, which was erroneously heated twice and cooled down faster over approximately 6 hours instead of 12 hours, yielded light-green, light-blue, dark-green, light-brown, and golden-brown products. Only the light-blue product was highly crystalline but single crystals of the light-green and golden-brown products were also found.

A picture taken of the product through an optical microscope is shown in Figure 3.1q.

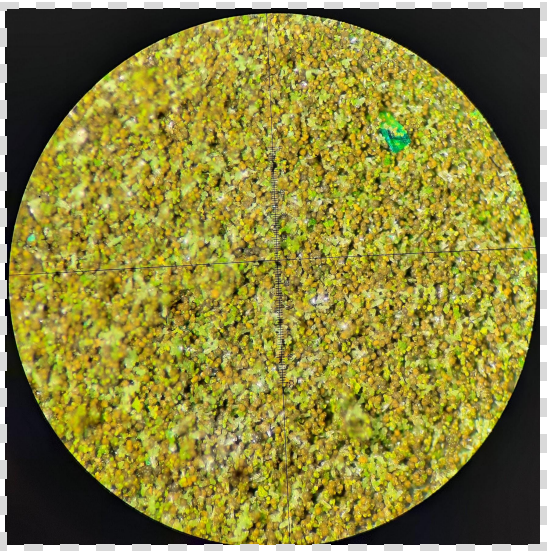

Figure 3.1q: Product obtained from Experiment 4. The picture was taken through an optical microscope but the exact scale is unknown.

3.1.3.1 Single Crystal X-ray diffraction

The light-green crystals were identified as the monoclinic polymorph of $CuSeO_3$. The structure was refined using crystals from *Experiment 1* and is shown in Figure 3.1b.

The light-blue crystals were identified as the orthorhombic $CuSeO_3 \cdot 2H_2O$. The structure was refined using crystals from *Experiment 1* and is shown in Figure 3.1c.

The golden-brown crystals were identified as the triclinic polymorph of $Cu_4O(SeO_3)_3$. The structure was refined using crystals from *Experiment 2* and is shown in Figure 3.1f.

3.1.3.2 Powder X-ray diffraction

Figure 3.1r shows the powder x-ray diffraction pattern of the ground-up bulk material, from which the light-blue $CuSeO_3 \cdot 2H_2O$ crystals had been removed. It was fitted using the monoclinic phase of $CuSeO_3$ (structure obtained from *Experiment 1*), cubic Cu_2OSeO_3 (structure obtained from *Experiment 2*), and monoclinic $Cu_4O(SeO_3)_3$ (structure obtained from the literature [2]. All the peak positions are accounted for using this three-phase model, but the peak intensities are not all well fitted, which is likely due to preferred orientation effects.

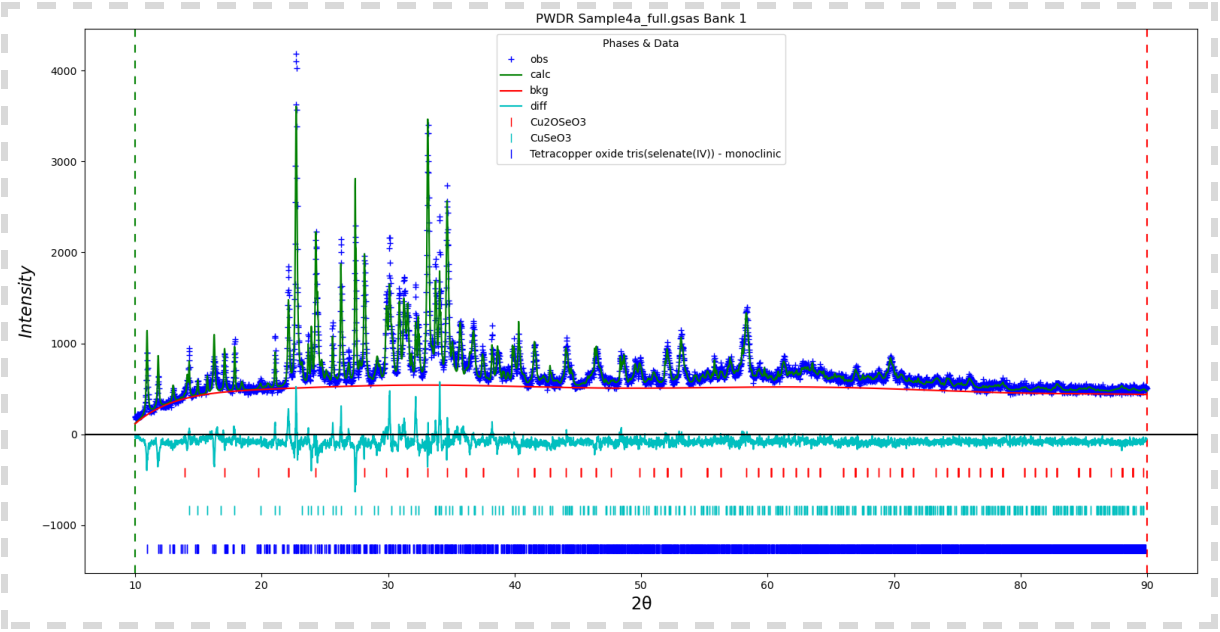

Figure 3.1r: Fitted powder x-ray diffraction pattern of the mixed products from Experiment 4.

3.1.4 Experiment 5 - 2:1 molar ratio

Experiment 5 with a 2:1 molar Cu:Se ratio yielded light-green, light-blue, dark-green, and red products.

The crystals had a noticeable amount of black powder coating their surfaces. Although no powder x-ray diffraction was done on this material, the black powder was likely leftover CuO, one of the two main reagents that is formed by decomposition of the starting material $Cu(OH)_2$ during the initial heating. A few red crystals identified as Cu_2O by single crystal x-ray diffraction were also present. The presence of these copper oxides can be explained by looking at the effects of product formation on the molar ratio of copper and selenium. The formation of $CuSeO_3$ in a preparation with copper excess will increase said excess, or put differently it will use up relatively more selenium. The formation of Cu_2OSeO_3 at a molar ratio of 2:1 will keep this molar ratio intact, although at higher copper excesses it will also increase this excess. There are no known copper selenides or selenites with a higher copper to selenium ratio than 2:1 that could form to use up the excess copper. Thus, these products will increase the copper excess until no more selenium is left, leaving behind CuO and allowing for the formation of Cu_2O.

A picture taken of the product through an optical microscope is shown in Figure 3.1s.

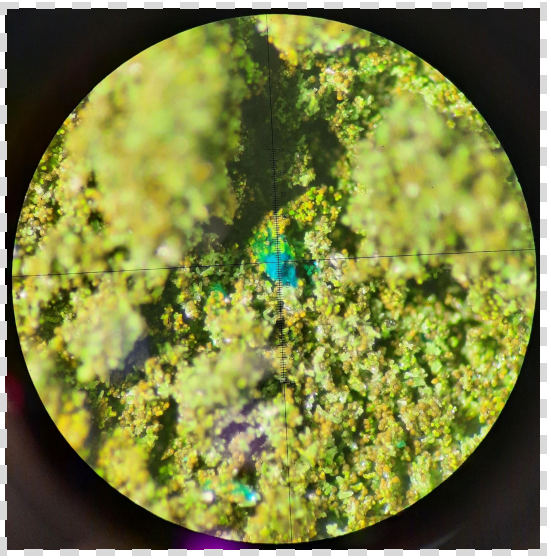

Figure 3.1s: Product obtained from Experiment 5. The picture was taken through an optical microscope but the exact scale is unknown.

3.1.4.1 Single Crystal X-ray diffraction

The light-green crystals were identified as the monoclinic polymorph of $CuSeO_3$. The structure was refined using crystals from *Experiment* 1 and is shown in Figure 3.1b.

The light-blue crystals were identified as the orthorhombic $CuSeO_3 \cdot 2H_2O$. The structure was refined using crystals from *Experiment* 1 and is shown in Figure 3.1c.

The dark-green crystals were identified as the cubic polymorph of Cu_2OSeO_3. The structure was refined using crystals from *Experiment* 2 and is shown in Figure 3.1k.

The red crystals were identified as Cu_2O, a well-known compound hence its structure was not refined.

3.1.5 Discussion

Experiment 1, 2, and 5 each included a product that would be expected considering the molar ratio of starting materials, $Cu(OH)_2$ and SeO_2. The 1:1 ratio yielded $CuSeO_3$ [$Cu_1Se_1O_3$], the 4:3 ratio yielded $Cu_4O(SeO_3)_3$ [$Cu_4Se_3O_{10}$], and the 2:1 ratio yielded Cu_2OSeO_3 [$Cu_2Se_1O_4$].

Monoclinic $CuSeO_3$ was formed in significant amounts in all hydrothermal syntheses. This can indicate that it is a kinetically favored product, allowing it to compete with other copper oxy-selenite compounds even at high excesses of copper.

To form cubic Cu_2OSeO_3 a copper excess was required. The 2:1 starting molar ratio [$Cu(OH)_2$: SeO_2] yielded the most of this product, but even the 4:3 and 3:2 starting molar ratios yielded significant amounts.

Only the starting molar ratio of 4:3 [$Cu(OH)_2$: SeO_2] yielded a significant amount of triclinic $Cu_4O(SeO_3)_3$, although it is likely that a starting molar ratio of 3:2 without reheating would also yield this product instead of the monoclinic polymorph. At higher copper excesses the formation of this product is suppressed by the formation of cubic Cu_2OSeO_3.

The formation of monoclinic $Cu_4O(SeO_3)_3$ with a 3:2 starting molar ratio [$Cu(OH)_2$: SeO_2] was unexpected, based on the formation of the triclinic polymorph with a 4:3 starting molar ratio. Although the faster cooling rate in this experiment was likely responsible for the mainly polycrystalline products, the accidental reheating procedure is suspected to have allowed the monoclinic phase to form.

Each hydrothermal synthesis also produced $CuSeO_3 \cdot 2H_2O$. This compound is not stable at the reaction temperature of 180℃, as per reports from the literature [27], and was thus likely formed during cooling from any leftover starting material.

Overall, it can be concluded that hydrothermal synthesis is a reliable and facile method for producing large batches of crystalline copper selenites and copper oxyselenites in a relatively short period of time. The monoclinic $CuSeO_3$ and cubic Cu_2OSeO_3 crystals were often stuck together in bulbous formations that were unsuitable for further analysis but thanks to the large amount of products formed there were enough suitable crystals, either single or twinned, for structural analysis using single crystal x-ray diffraction.

The main downside of using hydrothermal synthesis to produce these copper (oxy)selenite crystals is the lack of control over the specific products. Only the 1:1 starting molar ratio resulted in an almost uniform product of monoclinic $CuSeO_3$, the other syntheses having varying ratios of different products. This was usually not a problem for structural analysis using single crystal x-ray diffraction, for which suitable crystals were manually separated, but posed more of an issue for the magnetic measurements, for which larger numbers of individually small crystals had to be separated to obtain a high enough signal.

3.2 Chemical Vapor Transport Synthesis

3.2.1 Experiment 3 - 4:3 molar ratio

Experiment 3 with a 4:3 molar ratio of starting materials ($CuO:SeO_2$) yielded three different types of crystals. Green sheet- and needle-like crystals were found only at the very end (cold side) of the tube, whereas olive-green and dark red-brown sheet-like crystals were found growing in front of them. At the other end of the tube (hot side) a considerable amount of not transported and not crystallized black material had remained.

A picture taken of the product through an optical microscope is shown in *Figure 3.2a*.

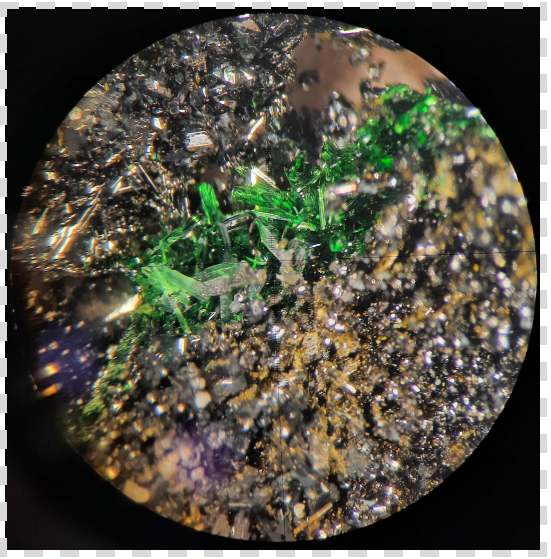

Figure 3.2a: Product obtained from Experiment 3. The picture was taken through an optical microscope but the exact scale is unknown.

3.2.1.1 Single Crystal X-ray diffraction

The green crystals were identified as the triclinic polymorph of $CuSeO_3$ with the $P\bar{1}$ space group, which is in agreement with previous literature reports [16]. The refined structure is shown in *Figure 3.2b*. Two of the four distinct copper cations are coordinated to five oxygens in a distorted square pyramidal configuration while the other two are coordinated to four oxygens in a planar geometry. All the selenium atoms are found in the form of SeO_3^{2-} anions. The structure contains multiple loops of corner-shared polyhedra consisting of both copper-oxygen-copper and copper-oxygen-selenium linkages. When looking at multiple unit cells a web-like structure appears with large tunnels going through the material along the *a*-axis, see Figure 3.2c. The structure bears no resemblance to its monoclinic polymorph, see Figure 3.2d.

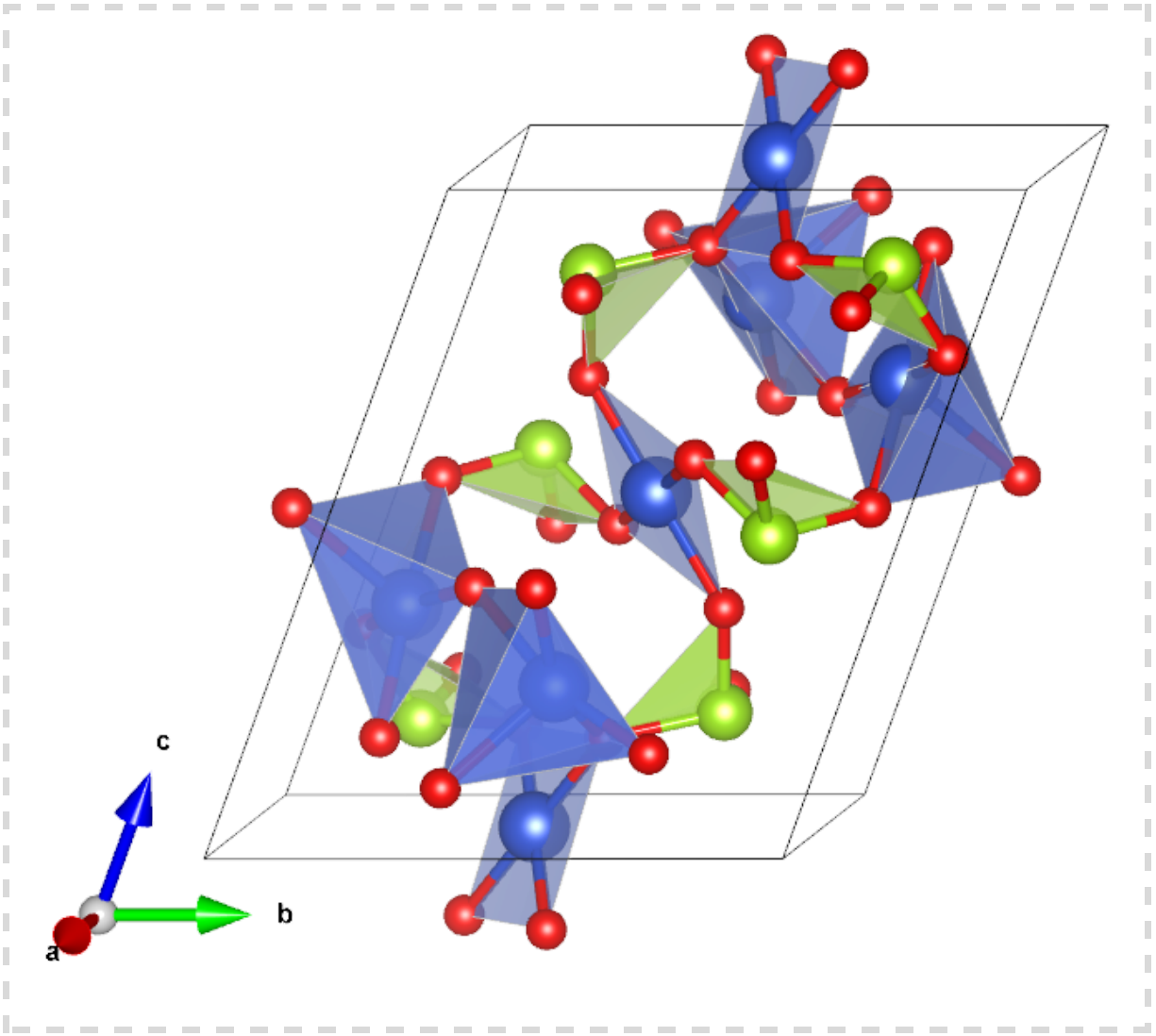

Figure 3.2b: Refined crystal structure of triclinic $CuSeO_3$.

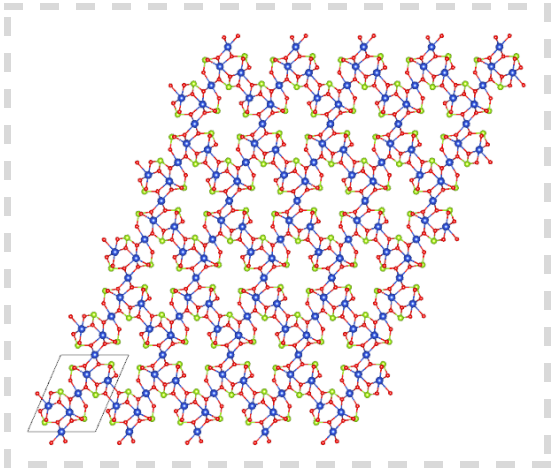

Figure 3.2c: Triclinic $CuSeO_3$ viewed along the b-c plane.

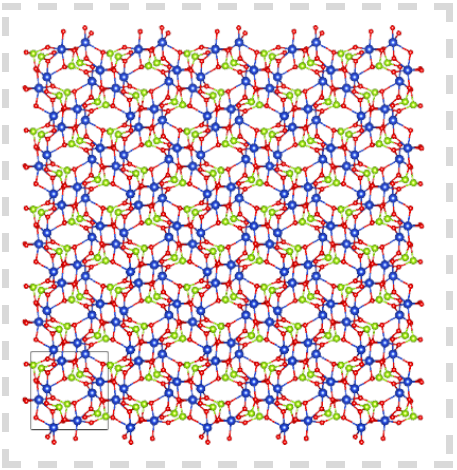

Figure 3.2d: Monoclinic $CuSeO_3$ viewed along the b-c plane.

The red-brown crystals were identified as $Cu_5O_2(SeO_3)_2Cl_2$ with the $P2_1/c$ space group, which is in agreement with previous literature reports [17]. The refined structure is shown in *Figure 3.2e*. The structure contains three distinct copper cations: one is coordinated to four oxygen anions in a planar geometry, one is coordinated to five oxygen anions and one chloride anion in an octahedral configuration, and one is coordinated to three oxygen anions and two chloride anions in a distorted square pyramidal configuration. All the selenium atoms are found in the form of SeO_3^{2-} anions. When looking at multiple unit cells, small tunnels going through the material along the *c* axis become visible, see *Figure 3.2g*.

The olive-green crystals were identified as $Cu_9O_2(SeO_3)_4Cl_6$ with the $P2_1/n$ space group, which is in agreement with previous literature reports [20]. The refined structure is shown in *Figure 3.2f*. Of the five distinct copper cations, one is coordinated to two oxygen and two chloride anions in a planar geometry, one is coordinated to four oxygen anions in a planar geometry, one is coordinated to four oxygen anions in a slightly distorted planar configuration, one is coordinated to two oxygen and two chloride anions in a slightly distorted planar configuration, and one is coordinated to four oxygen anions and one chloride anion in a distorted square pyramidal geometry. All the selenium atoms are found in the form of SeO_3^{2-} anions. When looking at multiple unit cells, small tunnels going through the material along the *b* axis become visible, see *Figure 3.2h*.

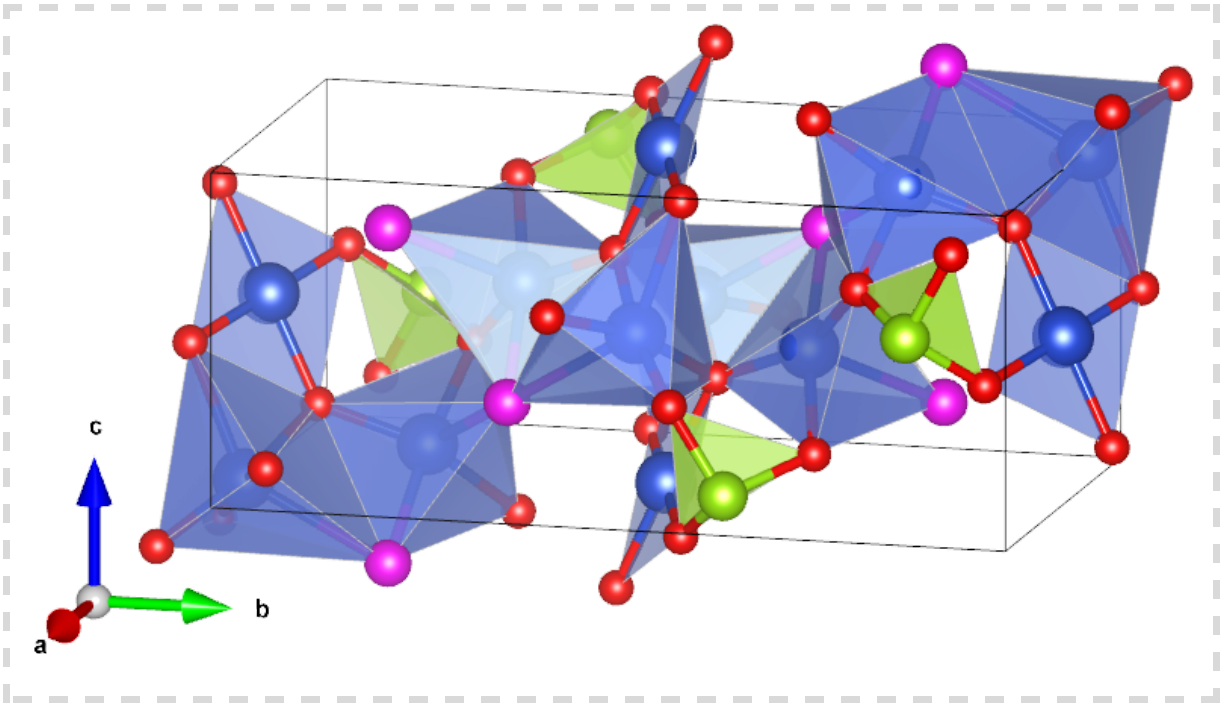

Figure 3.2e: Refined crystal structure of $Cu_5O_2(SeO_3)_2Cl_2$.

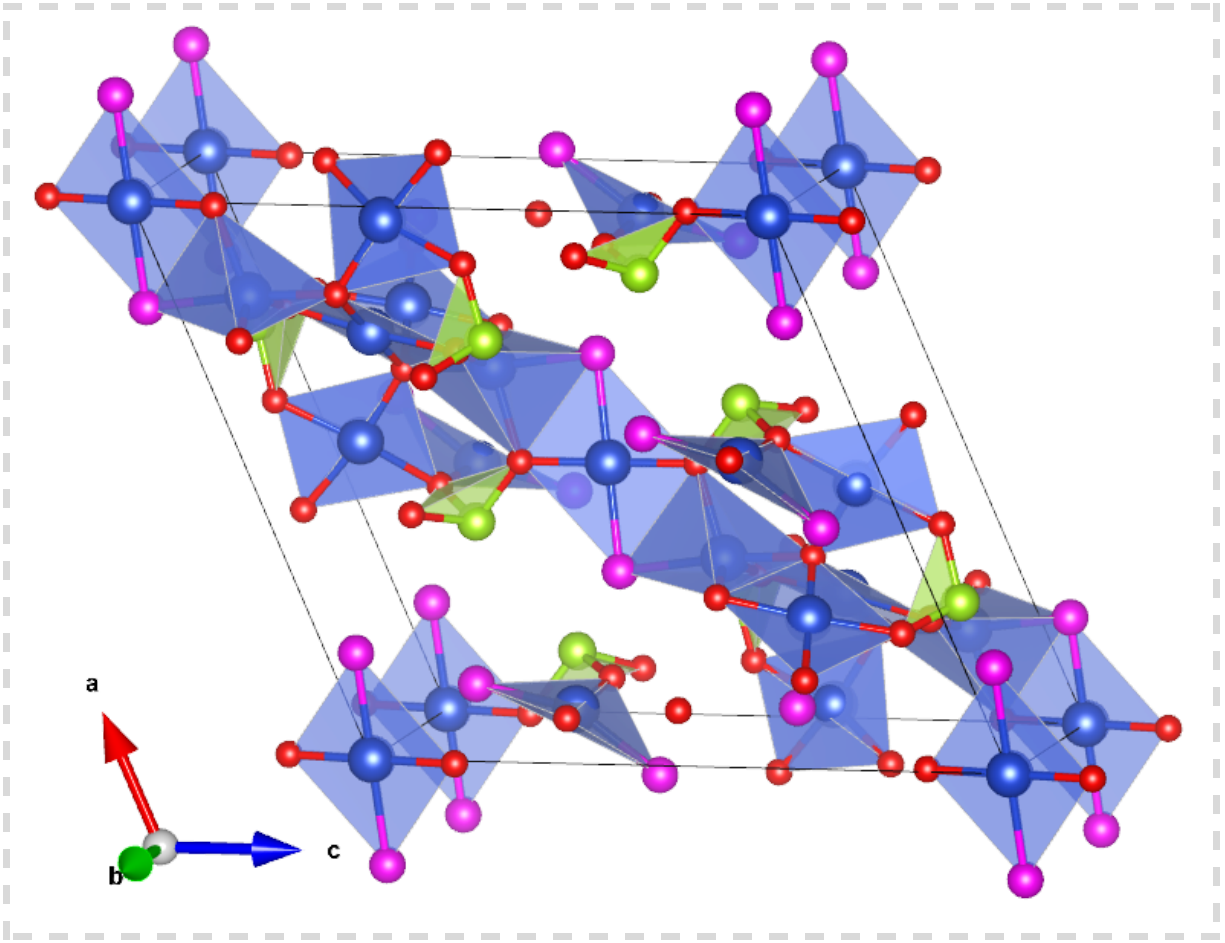

Figure 3.2f: Refined crystal structure of $Cu_9O_2(SeO_3)_4Cl_6$.

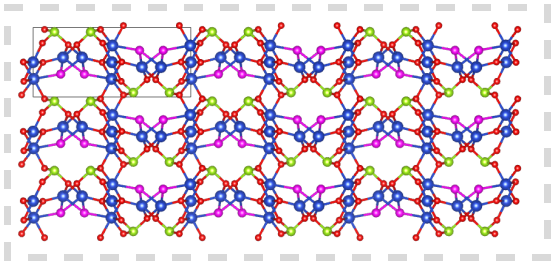

Figure 3.2g: $Cu_5O_2(SeO_3)_2Cl_2$ viewed along the a-b plane.

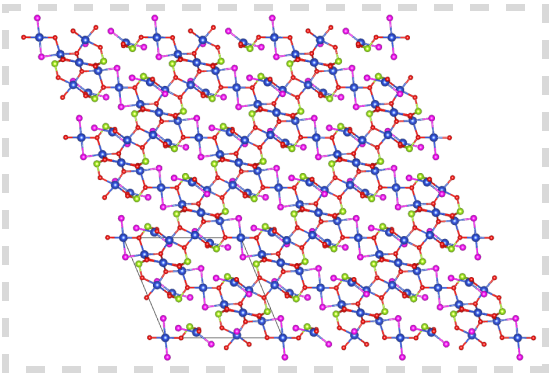

Figure 3.2h: $Cu_9O_2(SeO_3)_4Cl_6$ viewed along the a-c plane.

3.2.1.2 Powder X-ray diffraction

Figure 3.2i shows the powder x-ray diffraction pattern of the black polycrystalline material left behind at the hot end of the tube in *Experiment* 3 fitted using a CuO phase (structure obtained from the literature [32]). All peaks are accounted for and a final wRp value of 8.261% was obtained after refinement.

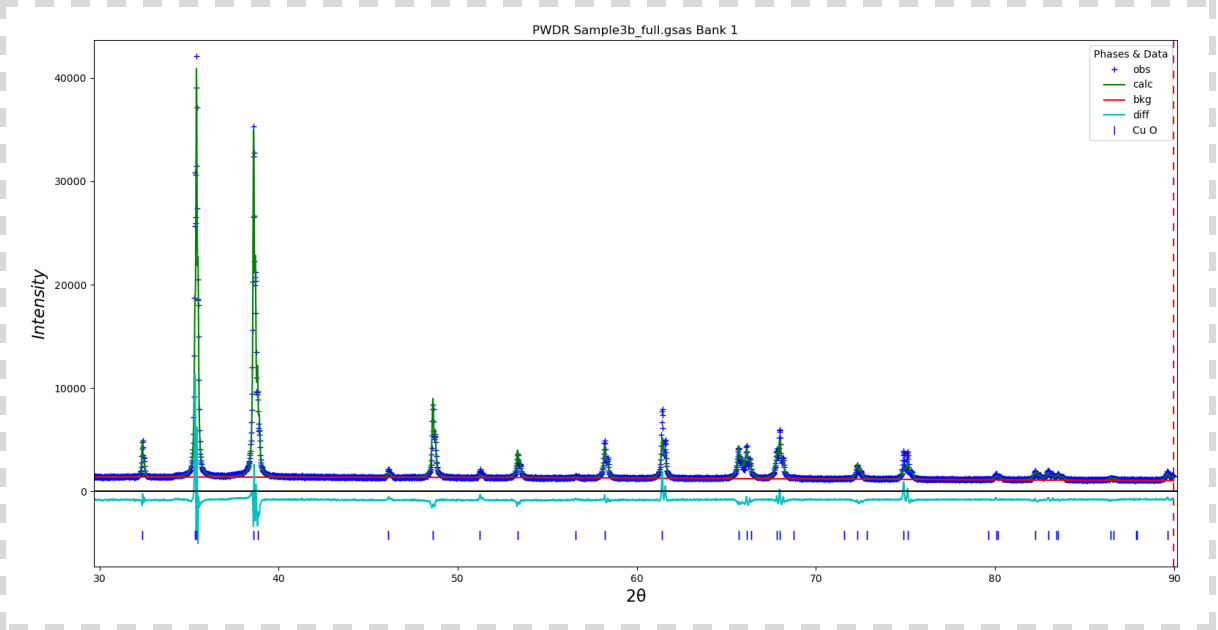

Figure 3.2i: Fitted powder x-ray diffraction pattern of black polycrystalline material left behind at the hot end of the tube in Experiment 3.

3.2.2 Experiment 6 - 2:1 molar ratio

Experiment 6 with a 2:1 molar ratio of Cu:Se yielded the same crystals of triclinic $CuSeO_3$, $Cu_5O_2(SeO_3)_2Cl_2$ and $Cu_9O_2(SeO_3)_4Cl_6$, as well as polycrystalline CuO. There was noticeably less crystalline product compared to *Experiment* 3.

A picture taken of the product through an optical microscope is shown in Figure 3.2j.

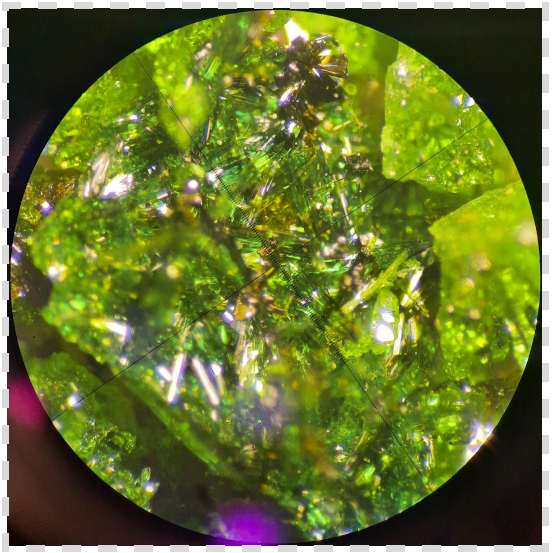

Figure 3.2j: Product obtained from Experiment 6. The picture was taken through an optical microscope but the exact scale is unknown.

3.2.3 Experiment 7 - 4:2 molar ratio

Experiment 7 with a 4:3 molar ratio of Cu:Se, half the amount of transport agent, and a larger temperature gradient, yielded dark-brown material and the same green crystalline product as in Experiments 3 and 6. The dark-brown material was mostly amorphous or polycrystalline but some small crystals were present. The materials were deposited considerably further up the tube compared to the previous two experiments.

A picture taken of the product through an optical microscope is shown in Figure 3.2k.

Figure 3.2k: Product obtained from Experiment 7. The picture was taken through an optical microscope but the exact scale is unknown.

3.2.3.1 Single Crystal X-ray diffraction

The green crystals were identified as the triclinic polymorph of $CuSeO_3$. The structure was refined using crystals from *Experiment* 3 and is shown in Figure 3.2b.

The dark-brown crystals were identified from the unit cell as the previously reported monoclinic phase of $Cu_4O(SeO_3)_3$; further structural analysis was not performed.

3.2.4 Discussion

All three chemical vapor transport syntheses yielded the triclinic phase of $CuSeO_3$ in the form of long green needle-like crystals upwards of 5 mm in length. These crystals were only found at the very end of the tube and thus must have been deposited only at the start of the reaction. This indicates either that the kinetics of $CuSeO_3$ formation are fast and/or that $CuSeO_3$ is favored by the transport agent.

The formation of $CuSeO_3$ also explains why substantial amounts of leftover CuO were still present at the end of the reactions as identified by powder x-ray diffraction for *Experiment* 3. For a 4:3 starting molar ratio of CuO and SeO_2 the formation of $CuSeO_3$ uses up relatively more selenium, causing an increasing excess of copper. As discussed in section 4.1, the hydrothermal reaction with the same starting molar ratio did not encounter this issue as Cu_2OSeO_3 was formed, which relative to a 4:3 ratio of copper and selenium uses up more copper and balances out the formation of $CuSeO_3$. Cu_2OSeO_3 was not present in any of the chemical vapor transport syntheses performed

and thus the selenium was used up leaving residual CuO. It is possible that this unbalanced reaction pathway played a role in the formation of the copper oxy-selenite chloride compounds.

These chloride compounds, $Cu_5O_2(SeO_3)_2Cl_2$ and $Cu_9O_2(SeO_3)_4Cl_6$, were formed in the first two chemical vapor transport syntheses instead of the expected phase $Cu_4O(SeO_3)_3$, indicating that reaction with the transport agent $SeCl_4$ occurred. To prevent these products from forming in the third chemical vapor transport synthesis, the amount of transport agent used was halved and the temperature gradient was increased. The reasoning was that in the first two attempts either the concentration of $SeCl_4$ was too high or the furnace was not able to maintain a stable temperature gradient, pushing the equilibrium at the colder end of the tube away from decomposition of the intermediate product into the product and the transport agent.

These changes resulted in the formation of the expected monoclinic phase of $Cu_4O(SeO_3)_3$ with only a few crystals of $Cu_5O_2(SeO_3)_2Cl_2$. Most of the transported dark-brown material appeared to be amorphous and the few crystals found were of low quality. They allowed only the lattice parameters to be determined and matched to those of monoclinic $Cu_4O(SeO_3)_3$ but the data were of too poor quality for a full structural solution. Increasing the temperature gradient also resulted in the deposition of material further up the quartz tube, as expected.

Overall, it can be concluded that chemical vapor transport synthesis is a reliable, albeit slow, method for producing relatively large and high quality single crystals of triclinic $CuSeO_3$. Although monoclinic $Cu_4O(SeO_3)_3$ was previously synthesized using this method [33], reproducing it proved difficult and likely requires more accurate temperature control to maintain an optimal temperature gradient.

4 Conclusion

Both hydrothermal and chemical vapor transport syntheses were successfully employed to obtain various crystals from the copper selenite and copper oxy-selenite families that were suitable for structural analysis using single crystal x-ray diffraction.

Triclinic $Cu_4O(SeO_3)_3$ crystals were successfully synthesized through hydrothermal synthesis using a 4:3 molar ratio of $Cu(OH)_2$ and SeO_2. Mixed products were obtained from this synthesis, consisting of roughly equal proportions of monoclinic $CuSeO_3$, cubic Cu_2OSeO_3, and triclinic $Cu_4O(SeO_3)_3$ single crystals, as well as a smaller number of $CuSeO_3 \cdot 2H_2O$ crystals. The quality of the triclinic $Cu_4O(SeO_3)_3$ crystals was consistently high compared to that of other copper selenite and copper oxy-selenite crystals, which often grew together in polycrystalline formations. The length of the rod shaped single crystals was in the 0.1mm range, which was insufficient for magnetic measurements. Large groups of single crystals had to be manually separated to perform temperature and field dependence measurements of the magnetisation.
Triclinic $Cu_4O(SeO_3)_3$ showed a primarily antiferromagnetic ordering with a Néel temperature around T=63K. This is argued to be a result of the arrangement of square pyramidal CuO_5 building blocks of which half are highly distorted towards a tetragonal bipyramidal configuration, giving rise to an antiparallel alignment of the spins which might be slightly rotated to give a small ferromagnetic moment.

Detailed field dependence measurements of the magnetisation were performed in the temperature and applied field ranges expected for a potential skyrmion phase but no evidence for such a phase was found.

Acknowledgements

I would like to thank Dr. Graeme Blake for taking time out of his busy schedule to supervise this project. Our meetings and discussions are always incredibly insightful. A thank you to Prof. Dr. Beatriz Noheda for being my second accessor. Your enthusiasm for your group and their work is very admirable. Lastly I would like to thank Jacob Baas for all his help with the experimental setup and measurements. Even sick at home you made sure I could do my scheduled measurements.

References

[1] Von Gattow V., "Die Kristallstruktur von $CuSeO_3.2H_2O$ (Chalkomenit)". *Acta Cryst* **11**, 377 (1958). https://doi.org/10.1107/S0365110X58001031.

[2] Effenberger H., Pertlik F., "Die Kristallstrukturen der Kupfer(II)-oxo-selenite $Cu_2O(SeO_3)$ (kubisch und monoklin) und $Cu_4O(SeO_3)_3$ (monoklin und triklin)". *Monatsh Chem* **117**, 887–896 (1986). https://doi.org/10.1007/BF00811258.

[3] Seki S., Yu X. Z., Ishiwata S., Tokura Y., "Observation of skyrmions in a multiferroic material". *Science* **336**, 198–201 (2012). https://doi.org/10.1126/science.1214143.

[4] Kang, Wang, Huang, Yangqi, Zhang, Xichao, Zhou, Yan. ZHAO, Weisheng, "Skyrmion-Electronics: An Overview and Outlook". *Proceedings of the IEEE.* **104**, 1-22 (2016). http://doi.org/10.1109/JPROC.2016.2591578.

[5] Lebech B., Bernhard J., Freltoft T., "Magnetic structures of cubic FeGe studied by small-angle neutron scattering". *J. Phys.: Condens. Matter* **1** 6105 (1989). https://doi.org/10.1088/0953-8984/1/35/010.

[6] Mühlbauer S., Binz B., Jonietz F., Pfleiderer C., Rosch A., Neubauer A., Georgii R., Böni P., "Skyrmion Lattice in a Chiral Magnet". *Science* **323**, 915-919 (2009). https://doi.org/10.1126/science.1166767.

[7] Leonov A. O., Monchesky T. L., Romming N., Kubetzka A., Bogdanov A. N., Wiesendanger R., "The properties of isolated chiral skyrmions in thin magnetic films". *New J. Phys.* **18** 065003 (2016). https://doi.org/10.1088/1367-2630/18/6/065003.

[8] Romming N., Hanneken C., Menzel M., Bickel J. E., Wolter B., Von Bergmann K., Kubetzka A., Wiesendanger R., "Writing and Deleting Single Magnetic Skyrmions". *Science* **341**, 636-639 (2013). https://doi.org/10.1126/science.1240573.

[9] Meyer, S., Perini, M., von Malottki, S. et al., "Isolated zero field sub-10 nm skyrmions in ultrathin Co films". *Nat Commun* **10** 3823 (2019). https://doi.org/10.1038/s41467-019-11831-4.

[10] Kurumaji T., Nakajima T., Hirschberger M., Kikkawa A., Yamasaki Y., Sagayama H., Nakao H., Taguchi Y., Arima T., Tokura Y., "Skyrmion lattice with a giant topological Hall effect in a frustrated triangular-lattice magnet". *Science* **365** 6456, 914-918 (2019). https://doi.org/10.1126/science.aau0968.

[11] Khanh N.D., Nakajima T., Yu X. et al., "Nanometric square skyrmion lattice in a centrosymmetric tetragonal magnet". *Nat. Nanotechnol.* **15**, 444–449 (2020). https://doi.org/10.1038/s41565-020-0684-7.

[12] Hirschberger M., Nakajima T., Gao S. et al., "Skyrmion phase and competing magnetic orders on a breathing kagomé lattice". *Nat. Commun.* **10** 5831 (2019). https://doi.org/10.1038/s41467-019-13675-4.

[13] Takagi R., Matsuyama N., Ukleev V. et al., "Square and rhombic lattices of magnetic skyrmions in a centrosymmetric binary compound". *Nat Commun* **13** 1472 (2022). https://doi.org/10.1038/s41467-022-29131-9.

[14] Hayami S., Motome Y., "Square skyrmion crystal in centrosymmetric itinerant magnets". *Phys. Rev. B* **103** 024439 (2020). https://doi.org/10.1103/PhysRevB.103.024439.

[15] Kohn K., Inoue K., Horie O., Akimoto S., "Crystal chemistry of MSeO3 and MTeO3 (M = Mg, Mn, Co, Ni, Cu, and Zn)". *Journal of Solid State Chemistry* **18**, 27-37 (1975). https://doi.org/10.1016/0022-4596(76)90075-X.

[16] Effenberger, H., "Die Kristallstrukturen von drei Modifikationen des $Cu(SeO_3)$". *Zeitschrift für Kristallographie - Crystalline Materials* **175**, 61-72 (1986). https://doi.org/10.1524/zkri.1986.175.14.61.

[17] Chandrasekhar Kakarla D., Yang Z. H., Wu H. C., Kuo T. W., Tiwari A., Li W.-H., Lee C. H., Wang Y.-Y., Lin J.-Y., Chang C. K., Chen B. H., Wang C.-W, Lee C. A., Chou M. M. C., Yang H. D., "Single crystal growth and structural, magnetic, and magnetoelectric properties in spin-frustrated bow-tie lattice of α-Cu5O2(SeO3)2Cl2". *Mater. Adv.* **24** (2021). http://dx.doi.org/10.1039/D1MA00526J.

[18] Vergasova L.P., Krivovichev S.V., Filatov S.K. et al., "Parageorgbokiite, β-Cu5O2(SeO3)2Cl2, a new mineral species from volcanic exhalations, Kamchatka Peninsula, Russia". *Geol. Ore Deposits* **49**, 518–521 (2007). https://doi.org/10.1134/S1075701507070057.

[19] "Crystal chemistry of inorganic compounds based on chains of oxocentered tetrahedra: I. Crystal structure of chloromenite, $Cu_9O_2(SeO_3)_4Cl_6$". *Zeitschrift für Kristallographie - Crystalline Materials*, **213**, 645-649 (1998). https://doi.org/10.1524/zkri.1998.213.12.645.
[20] Bastide B., Millet P., Johnsson M., Galy J., "Synthesis of copper(II) and selenium(IV) oxochlorides by chemical transport reaction: crystal structure of $Cu_9O_2(SeO_3)_4Cl_6$". *Materials Research Bulletin* **35**, 847-855 (2000). https://doi.org/10.1016/S0025-5408(00)00279-8.
[21] Wu H. C., Denisova K. N., Menzel D., Chandrasekhar Kakarla D., Maximova O. V., Kuo T. W., Yang Z. H., Lee C. H., Li W. H., Berger H., Wang C. W., Chang C. K., Chuang Y. C., Lin J.-Y., Gooch M., Chu C. W., Vasiliev A. N., Yang H. D., "Antiferroelectric antiferromagnetic type-I multiferroic Cu9O2(SeO3)4Cl6". *Phys. Rev. B* **100** 245119 (2019). https://doi.org/10.1103/PhysRevB.100.245119.
[22] Bos J.-W. G., Colin C., Palstra T., "Magnetoelectric coupling in the cubic ferrimagnet Cu2OSeO3". *Phys. Rev. B* **78** 094416 (2008). https://doi.org/10.1103/PhysRevB.78.094416.
[23] Belesi M., et al.., "Ferrimagnetism of the magnetoelectric compound Cu2OSeO3 probed by 77Se NMR". *Phys. Rev. B* **82** 094422 (2010). https://doi.org/10.1103/PhysRevB.82.094422.
[24] Malta J. F., Henriques M. S. C., Paixão J. A., Gonçalves A. P., "Magnetic studies of monoclinic Cu4O(SeO3)3, a copper-oxo-selenite derivative". *EPJ Web Conf.* **233** 01002 (2020). https://doi.org/10.1051/epjconf/202023301002.
[25] Živković I., Djokić D. M., Herak M., Pajić D., Prša K., Pattison P., Dominko D., Micković Z., Cinčić D., Forró L., Berger H., Rønnow H. M., "Site-selective quantum correlations revealed by magnetic anisotropy in the tetramer system SeCuO". *Phys. Rev. B* **86** 054405 (2012). http://dx.doi.org/10.1103/PhysRevB.86.054405.
[26] Tomar R., Kakkar S., Goyal S., Manolata Devi M., Bera C., Chakraverty S., "Multiple helimagnetic phases in triclinic CuSeO3". *Journal of Magnetism and Magnetic Materials* **497** 165945 (2020). https://doi.org/10.1016/j.jmmm.2019.165945.
[27] Larrañaga A., Mesa J. L., Lezama L., Arriortua M. I., Rojo T., "Mild Hydrothermal Synthesis of Cu(SeO3).2H2O: Structural Characterization, Thermal, Spectroscopic and Magnetic Studies". *Spectrochimica Acta Part A: Molecular and Biomolecular Spectroscopy* **72**, 356-360 (2009). https://doi.org/10.1016/j.saa.2008.10.032.
[28] Rabenau A., "The role of Hydrothermal Synthesis in Preparative Chemistry". *Angew. Chem. Int. Ed. Engl.* **24**, 1026-1040 (1985). https://doi.org/10.1002/anie.198510261.
[29] Binnewies M., Glaum R., Schmidt M., Schmidt P., "Chemical Vapor Transport Reactions – A Historical Review". *Z. anorg. allg. Chem.* **639**, 219 (2013). https://doi.org/10.1002/zaac.201300048.
[30] Gramm K., Lundgren L., Beckman O., "SQUID Magnetometer for Magnetization Measurements". *Physica Scripta* **13**, 93-95 (1976). http://doi.org/10.1088/0031-8949/13/2/004.
[31] Momma K., and Izumi F., "VESTA 3 for three-dimensional visualization of crystal, volumetric and morphology data". *J. Appl. Crystallogr.* **44**, 1272-1276 (2011). http://dx.doi.org/10.1107/S0021889811038970.
[32] Tunell G., Posnjak E., Ksanda, C. J., "Geometrical and Optical Properties, and Crystal Structure of Tenorite" *Zeitschrift für Kristallographie - Crystalline Materials* **90**, 120-142 (2015). https://doi.org/10.1524/zkri.1935.90.1.120.
[33] De Haas W. B., "Synthesis and investigation of copper-oxo-selenides". https://fse.studenttheses.ub.rug.nl/13648.

Supporting Material

Atom Tables

Monoclinic $CuSeO_3$

Atom	X	Y	Z
Cu01	0.47592(12)	0.20694(12)	0.52791(11)
Cu02	0.58399(13)	0.39786(13)	0.88411(11)
Se03	0.68599(8)	0.02786(9)	0.83030(8)
Se04	0.29900(9)	0.63471(9)	0.70901(8)
O05	0.7481(6)	0.2163(6)	0.9089(5)
O06	0.6593(6)	0.0616(6)	0.6314(5)
O07	0.8840(5)	-0.0635(6)	0.8434(5)
O08	0.4241(6)	0.5792(6)	0.8874(5)
O09	0.1202(6)	0.7199(6)	0.7682(6)
O10	0.4051(6)	0.7992(6)	0.6596(6)

Triclinic $CuSeO_3$

Atom	X	Y	Z
Cu01	0.0301(3)	0.50653(16)	0.74568(12)
Cu02	-0.500000	0.500000	0.500000
Cu03	0.500000	0.500000	1.000000
Cu04	0.4680(3)	0.85689(16)	0.66485(12)
Se05	-0.04218(17)	0.76930(11)	0.47836(8)
Se06	0.91982(18)	0.80709(11)	0.87878(9)
Se07	-0.47441(18)	0.24716(11)	0.83113(9)
O08	-0.5655(13)	0.3034(8)	0.6671(6)
O09	-0.1979(13)	0.5760(8)	0.5776(6)
O10	-0.1303(13)	0.2846(8)	0.8310(7)
O11	0.1941(12)	0.7227(8)	0.6131(6)
O12	0.7802(14)	0.9464(8)	0.7312(7)
O13	0.8104(13)	0.6169(8)	0.8762(6)

Atom	X	Y	Z
O14	-0.6210(12)	0.4221(8)	0.8563(6)
O15	-0.2853(12)	0.9020(8)	0.4971(6)
O16	1.2701(13)	0.8008(9)	0.8438(6)

Cubic Cu_2OSeO_3

Atom	X	Y	Z
Cu01	0.6214(2)	0.8710(2)	0.8836(2)
Cu02	0.6361(2)	0.6361(2)	0.6361(2)
Se03	0.96107(15)	0.96107(15)	0.96107(15)
Se04	0.29122(15)	0.79122(15)	0.70878(15)
O05	0.5119(9)	0.5119(9)	0.5119(9)
O06	0.4791(10)	0.7815(13)	0.7326(10)
O07	0.7816(11)	0.9366(10)	1.0193(10)
O08	0.7599(10)	0.7599(10)	0.7599(10)

Triclinic $Cu_4O(SeO_3)_3$

Atom	X	Y	Z
Cu01	0.82140(16)	0.44917(15)	0.10812(16)
Cu02	0.89584(17)	0.83859(14)	0.01534(16)
Cu03	0.59159(16)	0.56578(15)	0.75421(17)
Cu04	0.98655(16)	0.62830(15)	0.32430(15)
Se05	0.66278(11)	1.18811(10)	-0.02988(11)
Se06	0.44780(11)	0.28188(11)	0.62243(11)
Se07	0.90528(12)	0.79613(11)	0.66065(11)
O08	0.9684(7)	0.6147(7)	0.1056(7)
O09	0.4124(8)	0.4634(7)	0.7134(8)
O10	0.7358(8)	1.3477(7)	-0.2096(8)
O11	0.6431(7)	1.2925(7)	0.1328(7)
O12	0.2859(8)	0.3265(7)	0.5335(7)
O13	0.8713(8)	1.0801(7)	-0.0755(8)
O14	0.3524(8)	0.1356(7)	0.7997(8)

Atom	X	Y	Z
O15	1.0176(8)	0.6438(8)	0.5402(8)
O16	1.0423(8)	0.7955(7)	0.7686(8)
O17	0.7259(8)	0.6905(8)	0.8254(8)

Magnetic Measurement Sequences

ZFC and FC

```
>DAT DATAFILE "C:\QdMpms\Data\data2023\Pepijn\Copper_Selenides_Experiment2b_500oe_ZFC"
>LPT ScanTemp 5.000 70.000 66 1 0 1.000
>MRS MEASURERSO 5.000000 5 5 0 1 1 1 3 3 0 0 1 1 1 1
>ENT EOS
>LPT ScanTemp 72.000 180.000 55 1 0 2.000
>MRS MEASURERSO 5.000000 5 5 0 1 1 1 3 3 0 0 1 1 1 1
>ENT EOS
>LPT ScanTemp 185.000 300.000 24 1 0 5.000
>MRS MEASURERSO 5.000000 5 5 0 1 1 1 3 3 0 0 1 1 1 1
>ENT EOS
>DAT DATAFILE "C:\QdMpms\Data\data2023\Pepijn\Copper_Selenides_Experiment2b_500oe_FC"
>TMP TEMP 5.000 10.000
>WAI WAITFOR 240 0 1 299.9268 0 0
>LPT ScanTemp 5.000 70.000 66 1 0 1.000
>MRS MEASURERSO 5.000000 5 5 0 1 1 1 3 3 0 0 1 1 1 1
>ENT EOS
>LPT ScanTemp 72.000 180.000 55 1 0 2.000
>MRS MEASURERSO 5.000000 5 5 0 1 1 1 3 3 0 0 1 1 1 1
>ENT EOS
>LPT ScanTemp 185.000 300.000 24 1 0 5.000
>MRS MEASURERSO 5.000000 5 5 0 1 1 1 3 3 0 0 1 1 1 1
>ENT EOS
>TMP TEMP 100.000 10.000
>FLD FIELD 0.0 0 1
```

MH

```
>DAT DATAFILE "C:\QdMpms\Data\data2023\Pepijn\Measurement 2d\Copper_Selenides_Experiment2d_MH_10k"
>TMP TEMP 10.000 10.000
>WAI WAITFOR 240 0 1 138.4750 0 0
>LPB SCANB 0.00 1000.00 0 10 1 0
>MRS MEASURERSO 5.000000 5 3 0 1 1 1 3 3 0 0 1 1 1 1
>ENB EOS
>LPB SCANB 1500.00 10000.00 0 17 1 0
>MRS MEASURERSO 5.000000 5 3 0 1 1 1 3 3 0 0 1 1 1 1
>ENB EOS
>LPB SCANB 9500.00 1000.00 0 18 1 0
>MRS MEASURERSO 5.000000 5 3 0 1 1 1 3 3 0 0 1 1 1 1
>ENB EOS
>LPB SCANB 900.00 -1000.00 0 19 1 0
>MRS MEASURERSO 5.000000 5 3 0 1 1 1 3 3 0 0 1 1 1 1
>ENB EOS
>LPB SCANB -1500.00 -10000.00 0 17 1 0
>MRS MEASURERSO 5.000000 5 3 0 1 1 1 3 3 0 0 1 1 1 1
>ENB EOS
```

>LPB SCANB -9500.00 -1000.00 0 18 1 0
>MRS MEASURERSO 5.000000 5 3 0 1 1 1 3 3 0 0 1 1 1 1
>ENB EOS
>LPB SCANB -900.00 1000.00 0 19 1 0
>MRS MEASURERSO 5.000000 5 3 0 1 1 1 3 3 0 0 1 1 1 1
>ENB EOS
>LPB SCANB 1500.00 10000.00 0 17 1 0
>MRS MEASURERSO 5.000000 5 3 0 1 1 1 3 3 0 0 1 1 1 1
>ENB EOS
>FLD FIELD 0.0 0 0
>TMP TEMP 100.000 10.000
>DAT DATAFILE "C:\QdMpms\Data\data2023\Pepijn\Measurement 2d\Copper_Selenides_Experiment2d_MH_30k"
>TMP TEMP 30.000 10.000
>WAI WAITFOR 240 0 1 138.4750 0 0
>LPB SCANB 0.00 1000.00 0 10 1 0
>MRS MEASURERSO 5.000000 5 3 0 1 1 1 3 3 0 0 1 1 1 1
>ENB EOS
>LPB SCANB 1500.00 10000.00 0 17 1 0
>MRS MEASURERSO 5.000000 5 3 0 1 1 1 3 3 0 0 1 1 1 1
>ENB EOS
>LPB SCANB 9500.00 1000.00 0 18 1 0
>MRS MEASURERSO 5.000000 5 3 0 1 1 1 3 3 0 0 1 1 1 1
>ENB EOS
>LPB SCANB 900.00 -1000.00 0 19 1 0
>MRS MEASURERSO 5.000000 5 3 0 1 1 1 3 3 0 0 1 1 1 1
>ENB EOS
>LPB SCANB -1500.00 -10000.00 0 17 1 0
>MRS MEASURERSO 5.000000 5 3 0 1 1 1 3 3 0 0 1 1 1 1
>ENB EOS
>LPB SCANB -9500.00 -1000.00 0 18 1 0
>MRS MEASURERSO 5.000000 5 3 0 1 1 1 3 3 0 0 1 1 1 1
>ENB EOS
>LPB SCANB -900.00 1000.00 0 19 1 0
>MRS MEASURERSO 5.000000 5 3 0 1 1 1 3 3 0 0 1 1 1 1
>ENB EOS
>LPB SCANB 1500.00 10000.00 0 17 1 0
>MRS MEASURERSO 5.000000 5 3 0 1 1 1 3 3 0 0 1 1 1 1
>ENB EOS
>FLD FIELD 0.0 0 0
>DAT DATAFILE "C:\QdMpms\Data\data2023\Pepijn\Measurement 2d\Copper_Selenides_Experiment2d_MH_50k"
>TMP TEMP 50.000 10.000
>WAI WAITFOR 240 0 1 138.4750 0 0
>LPB SCANB 0.00 1000.00 0 10 1 0
>MRS MEASURERSO 5.000000 5 3 0 1 1 1 3 3 0 0 1 1 1 1
>ENB EOS
>LPB SCANB 1500.00 10000.00 0 17 1 0
>MRS MEASURERSO 5.000000 5 3 0 1 1 1 3 3 0 0 1 1 1 1
>ENB EOS
>LPB SCANB 9500.00 1000.00 0 18 1 0
>MRS MEASURERSO 5.000000 5 3 0 1 1 1 3 3 0 0 1 1 1 1
>ENB EOS
>LPB SCANB 900.00 -1000.00 0 19 1 0
>MRS MEASURERSO 5.000000 5 3 0 1 1 1 3 3 0 0 1 1 1 1
>ENB EOS
>LPB SCANB -1500.00 -10000.00 0 17 1 0
>MRS MEASURERSO 5.000000 5 3 0 1 1 1 3 3 0 0 1 1 1 1
>ENB EOS
>LPB SCANB -9500.00 -1000.00 0 18 1 0
>MRS MEASURERSO 5.000000 5 3 0 1 1 1 3 3 0 0 1 1 1 1

>ENB EOS
>LPB SCANB -900.00 1000.00 0 19 1 0
>MRS MEASURERSO 5.000000 5 3 0 1 1 1 3 3 0 0 1 1 1 1
>ENB EOS
>LPB SCANB 1500.00 10000.00 0 17 1 0
>MRS MEASURERSO 5.000000 5 3 0 1 1 1 3 3 0 0 1 1 1 1
>ENB EOS
>FLD FIELD 0.0 0 0
>DAT DATAFILE "C:\QdMpms\Data\data2023\Pepijn\Measurement 2d\Copper_Selenides_Experiment2d_MH_60k"
>TMP TEMP 60.000 10.000
>WAI WAITFOR 240 0 1 138.4750 0 0
>LPB SCANB 0.00 1000.00 0 10 1 0
>MRS MEASURERSO 5.000000 5 3 0 1 1 1 3 3 0 0 1 1 1 1
>ENB EOS
>LPB SCANB 1500.00 10000.00 0 17 1 0
>MRS MEASURERSO 5.000000 5 3 0 1 1 1 3 3 0 0 1 1 1 1
>ENB EOS
>LPB SCANB 9500.00 1000.00 0 18 1 0
>MRS MEASURERSO 5.000000 5 3 0 1 1 1 3 3 0 0 1 1 1 1
>ENB EOS
>LPB SCANB 900.00 -1000.00 0 19 1 0
>MRS MEASURERSO 5.000000 5 3 0 1 1 1 3 3 0 0 1 1 1 1
>ENB EOS
>LPB SCANB -1500.00 -10000.00 0 17 1 0
>MRS MEASURERSO 5.000000 5 3 0 1 1 1 3 3 0 0 1 1 1 1
>ENB EOS
>LPB SCANB -9500.00 -1000.00 0 18 1 0
>MRS MEASURERSO 5.000000 5 3 0 1 1 1 3 3 0 0 1 1 1 1
>ENB EOS
>LPB SCANB -900.00 1000.00 0 19 1 0
>MRS MEASURERSO 5.000000 5 3 0 1 1 1 3 3 0 0 1 1 1 1
>ENB EOS
>LPB SCANB 1500.00 10000.00 0 17 1 0
>MRS MEASURERSO 5.000000 5 3 0 1 1 1 3 3 0 0 1 1 1 1
>ENB EOS
>FLD FIELD 0.0 0 0
>TMP TEMP 100.000 10.000
>DAT DATAFILE "C:\QdMpms\Data\data2023\Pepijn\Measurement 2e\Copper_Selenides_Experiment2e_MH_52k"
>TMP TEMP 52.000 10.000
>WAI WAITFOR 240 0 1 138.4750 0 0
>LPB SCANB 0.00 1000.00 0 100 1 0
>MRS MEASURERSO 5.000000 5 3 0 1 1 1 3 3 0 0 1 1 1 1
>ENB EOS
>DAT DATAFILE "C:\QdMpms\Data\data2023\Pepijn\Measurement 2e\Copper_Selenides_Experiment2e_MH_52.5k"
>TMP TEMP 52.500 10.000
>FLD FIELD 0.0 0 0
>LPB SCANB 0.00 1000.00 0 100 1 0
>MRS MEASURERSO 5.000000 5 3 0 1 1 1 3 3 0 0 1 1 1 1
>ENB EOS
>DAT DATAFILE "C:\QdMpms\Data\data2023\Pepijn\Measurement 2e\Copper_Selenides_Experiment2e_MH_53k"
>TMP TEMP 53.000 10.000
>FLD FIELD 0.0 0 0
>LPB SCANB 0.00 1000.00 0 100 1 0
>MRS MEASURERSO 5.000000 5 3 0 1 1 1 3 3 0 0 1 1 1 1
>ENB EOS
>DAT DATAFILE "C:\QdMpms\Data\data2023\Pepijn\Measurement 2e\Copper_Selenides_Experiment2e_MH_53.5k"
>TMP TEMP 53.500 10.000
>FLD FIELD 0.0 0 0
>LPB SCANB 0.00 1000.00 0 100 1 0

>MRS MEASURERSO 5.000000 5 3 0 1 1 1 3 3 0 0 1 1 1 1
>ENB EOS
>DAT DATAFILE "C:\QdMpms\Data\data2023\Pepijn\Measurement 2e\Copper_Selenides_Experiment2e_MH_54k"
>TMP TEMP 54.000 10.000
>FLD FIELD 0.0 0 0
>LPB SCANB 0.00 1000.00 0 100 1 0
>MRS MEASURERSO 5.000000 5 3 0 1 1 1 3 3 0 0 1 1 1 1
>ENB EOS
>DAT DATAFILE "C:\QdMpms\Data\data2023\Pepijn\Measurement 2e\Copper_Selenides_Experiment2e_MH_54.5k"
>TMP TEMP 54.500 10.000
>FLD FIELD 0.0 0 0
>LPB SCANB 0.00 1000.00 0 100 1 0
>MRS MEASURERSO 5.000000 5 3 0 1 1 1 3 3 0 0 1 1 1 1
>ENB EOS
>DAT DATAFILE "C:\QdMpms\Data\data2023\Pepijn\Measurement 2e\Copper_Selenides_Experiment2e_MH_55k"
>TMP TEMP 55.000 10.000
>FLD FIELD 0.0 0 0
>LPB SCANB 0.00 1000.00 0 100 1 0
>MRS MEASURERSO 5.000000 5 3 0 1 1 1 3 3 0 0 1 1 1 1
>ENB EOS
>DAT DATAFILE "C:\QdMpms\Data\data2023\Pepijn\Measurement 2e\Copper_Selenides_Experiment2e_MH_55.5k"
>TMP TEMP 55.500 10.000
>FLD FIELD 0.0 0 0
>LPB SCANB 0.00 1000.00 0 100 1 0
>MRS MEASURERSO 5.000000 5 3 0 1 1 1 3 3 0 0 1 1 1 1
>ENB EOS
>DAT DATAFILE "C:\QdMpms\Data\data2023\Pepijn\Measurement 2e\Copper_Selenides_Experiment2e_MH_56k"
>TMP TEMP 56.000 10.000
>FLD FIELD 0.0 0 0
>LPB SCANB 0.00 1000.00 0 100 1 0
>MRS MEASURERSO 5.000000 5 3 0 1 1 1 3 3 0 0 1 1 1 1
>ENB EOS
>DAT DATAFILE "C:\QdMpms\Data\data2023\Pepijn\Measurement 2e\Copper_Selenides_Experiment2e_MH_56.5k"
>TMP TEMP 56.500 10.000
>FLD FIELD 0.0 0 0
>LPB SCANB 0.00 1000.00 0 100 1 0
>MRS MEASURERSO 5.000000 5 3 0 1 1 1 3 3 0 0 1 1 1 1
>ENB EOS
>DAT DATAFILE "C:\QdMpms\Data\data2023\Pepijn\Measurement 2e\Copper_Selenides_Experiment2e_MH_57k"
>TMP TEMP 57.000 10.000
>FLD FIELD 0.0 0 0
>LPB SCANB 0.00 1000.00 0 100 1 0
>MRS MEASURERSO 5.000000 5 3 0 1 1 1 3 3 0 0 1 1 1 1
>ENB EOS
>DAT DATAFILE "C:\QdMpms\Data\data2023\Pepijn\Measurement 2e\Copper_Selenides_Experiment2e_MH_57.5k"
>TMP TEMP 57.500 10.000
>FLD FIELD 0.0 0 0
>LPB SCANB 0.00 1000.00 0 100 1 0
>MRS MEASURERSO 5.000000 5 3 0 1 1 1 3 3 0 0 1 1 1 1
>ENB EOS
>DAT DATAFILE "C:\QdMpms\Data\data2023\Pepijn\Measurement 2e\Copper_Selenides_Experiment2e_MH_58k"
>TMP TEMP 58.000 10.000
>FLD FIELD 0.0 0 0
>LPB SCANB 0.00 1000.00 0 100 1 0
>MRS MEASURERSO 5.000000 5 3 0 1 1 1 3 3 0 0 1 1 1 1
>ENB EOS
>DAT DATAFILE "C:\QdMpms\Data\data2023\Pepijn\Measurement 2e\Copper_Selenides_Experiment2e_MH_58.5k"
>TMP TEMP 58.500 10.000
>FLD FIELD 0.0 0 0

```
>LPB SCANB 0.00 1000.00 0 100 1 0
>MRS MEASURERSO 5.000000 5 3 0 1 1 1 3 3 0 0 1 1 1 1
>ENB EOS
>DAT DATAFILE "C:\QdMpms\Data\data2023\Pepijn\Measurement 2e\Copper_Selenides_Experiment2e_MH_59k"
>TMP TEMP 59.000 10.000
>FLD FIELD 0.0 0 0
>LPB SCANB 0.00 1000.00 0 100 1 0
>MRS MEASURERSO 5.000000 5 3 0 1 1 1 3 3 0 0 1 1 1 1
>ENB EOS
>DAT DATAFILE "C:\QdMpms\Data\data2023\Pepijn\Measurement 2e\Copper_Selenides_Experiment2e_MH_59.5k"
>TMP TEMP 59.500 10.000
>FLD FIELD 0.0 0 0
>LPB SCANB 0.00 1000.00 0 100 1 0
>MRS MEASURERSO 5.000000 5 3 0 1 1 1 3 3 0 0 1 1 1 1
>ENB EOS
>DAT DATAFILE "C:\QdMpms\Data\data2023\Pepijn\Measurement 2e\Copper_Selenides_Experiment2e_MH_60k"
>TMP TEMP 60.000 10.000
>FLD FIELD 0.0 0 0
>LPB SCANB 0.00 1000.00 0 100 1 0
>MRS MEASURERSO 5.000000 5 3 0 1 1 1 3 3 0 0 1 1 1 1
>ENB EOS
>FLD FIELD 0.0 0 0
>TMP TEMP 100.000 10.000
```